iScience

CellPress
OPEN ACCESS

Article

Activation of amino acid metabolic program in cardiac HIF1-alpha-deficient mice

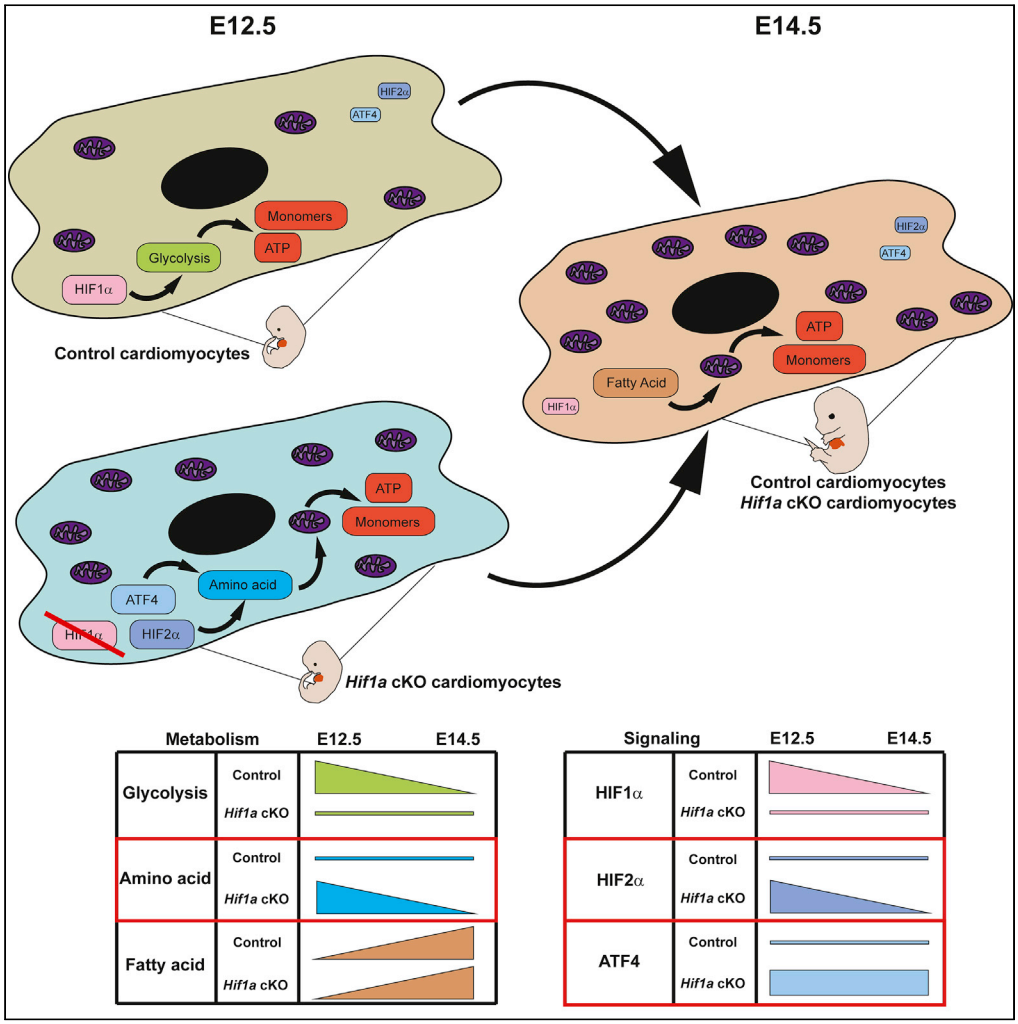

Ivan Menendez-Montes, Beatriz Escobar, Manuel J. Gomez, ..., Jesus Ruiz-Cabello, Jesus Vázquez, Silvia Martin-Puig

silvia.martin@cnic.es, silvia.martin@ufv.es

HIGHLIGHTS

Loss of cardiac *Hif1a* does not preclude heart development or cardiac function

Embryonic *Hif1a*-deficient hearts transiently upregulate amino acid catabolism

Amino acid catabolism activation sustains heart growth in the absence of glycolysis

HIF2α and ATF4 are transiently upregulated in the developing heart upon *Hif1a* loss

Menendez-Montes et al., iScience *24*, 102124 February 19, 2021
https://doi.org/10.1016/j.isci.2021.102124

iScience

CellPress
OPEN ACCESS

Article

Activation of amino acid metabolic program in cardiac HIF1-alpha-deficient mice

Ivan Menendez-Montes,[1,2] Beatriz Escobar,[1] Manuel J. Gomez,[3] Teresa Albendea-Gomez,[1,4] Beatriz Palacios,[1] Elena Bonzon-Kulichenko,[5] Jose Luis Izquierdo-Garcia,[6,7,8] Ana Vanessa Alonso,[9] Alessia Ferrarini,[5] Luis Jesus Jimenez-Borreguero,[9,10] Jesus Ruiz-Cabello,[6,7,8,11] Jesus Vázquez,[5,12] and Silvia Martin-Puig[1,4,13,*]

SUMMARY

HIF1-alpha expression defines metabolic compartments in the developing heart, promoting glycolytic program in the compact myocardium and mitochondrial enrichment in the trabeculae. Nonetheless, its role in cardiogenesis is debated. To assess the importance of HIF1-alpha during heart development and the influence of glycolysis in ventricular chamber formation, herein we generated conditional knockout models of *Hif1a* in Nkx2.5 cardiac progenitors and cardiomyocytes. Deletion of *Hif1a* impairs embryonic glycolysis without influencing cardiomyocyte proliferation and results in increased mitochondrial number and transient activation of amino acid catabolism together with HIF2α and ATF4 upregulation by E12.5. *Hif1a* mutants display normal fatty acid oxidation program and do not show cardiac dysfunction in the adulthood. Our results demonstrate that cardiac HIF1 signaling and glycolysis are dispensable for mouse heart development and reveal the metabolic flexibility of the embryonic myocardium to consume amino acids, raising the potential use of alternative metabolic substrates as therapeutic interventions during ischemic events.

INTRODUCTION

The heart is the first organ to form *in utero*, and it is essential to deliver oxygen and nutrients to embryonic tissues from early stages of development. Different subsets of cardiac progenitors proliferate, migrate, and differentiate into the diverse cell types that form the mature heart (Martin-Puig et al., 2008; Watanabe and Buckingham, 2010). Nkx2.5 cardiovascular progenitors give rise to the majority of cardiac cells, contributing to epicardium, myocardium, and endocardium (Moses et al., 2001). Cardiogenesis is a complex process that can result in malformations, and congenital heart defects occur in 1% of live births. Several factors have been involved in developmental cardiac failure, and among them hypoxia has been previously described as an environmental factor associated with cardiac defects during pregnancy (Cerychova and Pavlinkova, 2018; Nanka et al., 2008). Hypoxia-inducible factors (HIFs) are known to mediate a well-characterized transcriptional response to low oxygen tensions. HIF heterodimers are formed by a constitutively expressed β subunit (HIFβ or ARNT) and an oxygen-regulated α subunit, with three different isoforms (1α, 2α, and 3α) (Kaelin and Ratcliffe, 2008). Under normoxic conditions, the oxygen sensors prolyl hydroxylases (PHDs) hydroxylate HIFα in specific proline residues (Jiang et al., 1997). These modifications are recognized by the von Hippel-Lindau/E3 ubiquitin ligase complex, which polyubiquitinates and drives α subunits to proteasomal degradation. In hypoxic conditions, α subunits evade degradation due to the inhibited PHD activity, dimerize with β subunits, and mediate the adaptive response to hypoxia by activating the transcription of their target genes (Pouyssegur et al., 2006).

Poorly oxygenated areas appear during heart development (Lee et al., 2001) and physiological hypoxia is involved in outflow tract remodeling (Sugishita et al., 2004). However, chronic exposure of pregnant females to low oxygen causes embryonic myocardial thinning and epicardial detachment (Menendez-Montes et al., 2016; Ream et al., 2008) and excessive embryonic hypoxia also increases the vulnerability to suffer common septation and conotruncal heart defects (Kenchegowda et al., 2014). Genetic-based overactivation of HIF signaling by inactivation of *Vhl* in cardiac progenitors using different drivers (Mlc2vCre, Nkx2.5Cre) causes morphological, metabolic, and functional cardiac alterations that result in embryonic lethality (Lei et al., 2008; Menendez-Montes et al., 2016). On the other hand, *Hif1a* conditional

[1]Myocardial Pathophysiology Area. National Center for Cardiovascular Research, Melchor Fernandez Almagro 3, 28029 Madrid, Spain

[2]Department of Internal Medicine, University of Texas Southwestern Medical Center, Dallas, TX, USA

[3]Bioinformatics Unit. National Center for Cardiovascular Research. Madrid, Spain

[4]Facultad de Medicina. Universidad Francisco de Vitoria, Madrid, Spain

[5]Vascular Pathophysiology Area. National Center for Cardiovascular Research. Madrid, Spain

[6]Center for Cooperative Research in Biomaterials (CIC biomaGUNE), Basque Research and Technology Alliance (BRTA), 20014 Donostia San Sebastián, Spain

[7]CIBER de Enfermedades Respiratorias (CIBERES), 28029 Madrid, Spain

[8]Departamento de Química en Ciencias Farmaceuticas. Facultad de Farmacia, Universidad Complutense de Madrid, 28040 Madrid, Spain

[9]Advanced Imaging Unit. National Center for Cardiovascular Research. Madrid, Spain

[10]Cardiology Unit, Hospital Universitario de La Princesa, Madrid, Spain

[11]IKERBASQUE, Basque Foundation for Science, 48013 Bilbao, Spain

[12]CIBER de Enfermedades Cardiovasculares (CIBERCV), Madrid, Spain

[13]Lead contact

*Correspondence: silvia.martin@cnic.es, silvia.martin@ufv.es

https://doi.org/10.1016/j.isci.2021.102124

loss-of-function models in cardiac progenitors and cardiomyocytes also causes several embryonic cardiac alterations (Guimarães-Camboa et al., 2015; Huang et al., 2004; Krishnan et al., 2008), suggesting that a controlled balance in oxygen levels and hypoxia signaling is required for proper cardiac development. However, important phenotypic discrepancies between the different published loss-of-function models exist. On one hand, the use of cardiac-specific Mlc2vCre driver in combination with a *Hif1a* floxed mice does not affect embryonic survival but causes cardiac hypertrophy with reduced cardiac function in the adulthood, together with decreased glycolysis and ATP and lactate levels (Huang et al., 2004). On the other hand, when a null *Hif1a* allele in germline is used in combination with a *Hif1a* floxed allele and the Mlc2vCre driver, mutant embryos show several cardiac alterations and increased cardiomyocyte proliferation, with associated embryonic lethality by E12.0 (Krishnan et al., 2008). The combination of null and floxed *Hif1a* alleles under the control of Nkx2.5Cre driver provides a more homogeneous recombination than Mlc2vCre and results in the activation of cell stress pathways that inhibit cardiomyocyte proliferation and lead to myocardial thinning, resulting in embryonic lethality by E15.5 (Guimarães-Camboa et al., 2015). Considering the importance of hypoxia pathway in early hematopoiesis, placentation, and vascular development (Llurba Olive et al., 2018), the potential secondary effect of using *Hif1a*-null alleles on cardiac development cannot be ruled out when interpreting data from some of these mutants. Therefore, although it is clear that sustained HIF1 signaling in the embryonic heart is detrimental for proper cardiac development, there is still disagreement and open debate about the impact of Hif1a loss during cardiogenesis and subsequent effects on cardiac function.

HIF1 signaling is an important regulator of cellular metabolism in physiological and pathological contexts. In addition to glycolytic activation (Majmundar et al., 2010), HIF1 reduces mitochondrial metabolism by repressing pyruvate entry into the mitochondria (Kim et al., 2006) and by promoting COX4 isoform switch from COX4-1 to COX4-2 (Fukuda et al., 2007). Moreover, HIF1 can also limit oxidative metabolism through an inhibitory role on mitochondrial biogenesis (Zhang et al., 2007). Several *in vitro* studies have demonstrated that the embryonic heart relies on glycolysis for energy supply (Chung et al, 2010, 2011), in contrast with the adult heart that sustains most of ATP production through mitochondrial oxidation of fatty acids (FA) (Lopaschuk and Jaswal, 2010). This metabolic switch is coincident with the change in oxygen levels after birth (Puente et al., 2014). However, a recent report from our group has shown that an earlier metabolic shift toward FA oxidation occurs during development at around E14.5, through a mechanism dependent on a decrease in HIF1 signaling in the embryonic myocardium (Menendez-Montes et al., 2016). Despite the importance of glucose and FAs as cardiac energy sources, amino acids can also be used as bioenergetics fuel. Hence, amino acids have the capacity to enter the Krebs Cycle at different levels, a phenomenon known as anaplerosis, and to replenish metabolic intermediates that warrant both NADH/$FADH_2$ and building blocks production that enable the cells to continue growing under amino acid metabolism. The importance of amino acids as catabolic substrates has been described in tumor growth (Yue et al., 2017), pulmonary hypertension (Piao et al., 2013), or limited oxygen supply conditions (Bing et al., 1954; Julia et al., 1990). However, the ability of the embryonic heart to catabolize amino acids remains unexplored.

Herein, we describe that *Hif1a* loss in Nkx2.5 cardiovascular progenitors or cardiomyocytes during heart development blunts glycolysis and drives a compensatory metabolic adaptation based on transient activation of amino acid transport and catabolism associated with increased ATF4 and HIF2α to maintain energy production and growth. Our results demonstrate that HIF1 signaling in Nkx2.5 progenitors and cardiomyocytes is dispensable for cardiogenesis and show the relevance of amino acid metabolism during cardiac development in the absence of glycolysis, opening future research horizons toward studying the ability of the heart to use amino acids as an alternative energy fuel and biosynthetic precursor source in different pathophysiological contexts like cardiac ischemia and regeneration.

RESULTS

HIF1 signaling in Nkx2.5 progenitors is dispensable for cardiac development

HIF1α is expressed in the developing myocardium, with a temporal dynamics along midgestation (Guimarães-Camboa et al., 2015; Krishnan et al., 2008; Menendez-Montes et al., 2016). We and others have described the heterogeneous regional distribution of HIF1 signaling with high HIF1α levels in the compact myocardium in contrast with low expression in the trabeculae (Guimarães-Camboa et al., 2015; Menendez-Montes et al., 2016). To investigate the role of HIF1 in heart development we generated a cardiac-specific loss-of-function model using two floxed alleles of *Hif1a* gene in combination with the cardiac

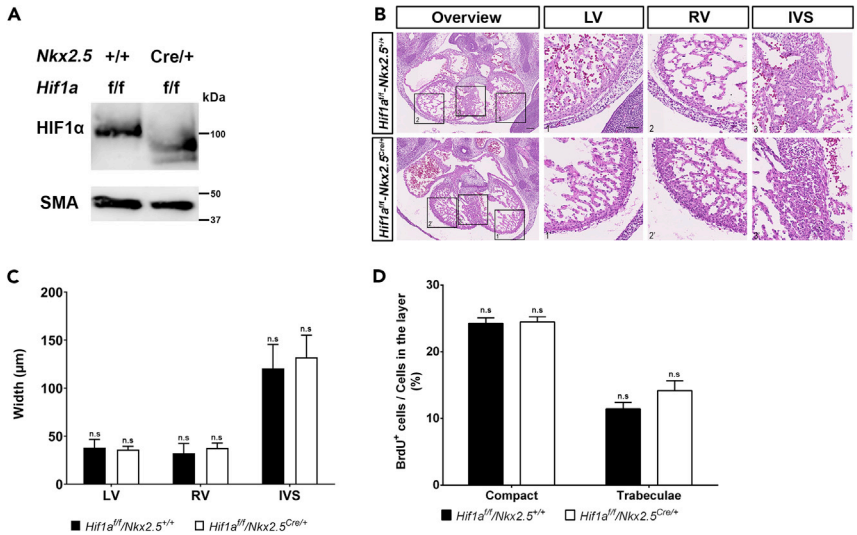

Figure 1. Embryonic phenotype of *Hif1a*-deficient embryos at E12.5

(A) Representative immunoblot against HIF1α (upper panel) and smooth muscle actin (SMA, lower panel) in heart lysates of control (*Hif1a*$^{f/f}$/*Nkx2.5*$^{+/+}$) and *Hif1a*/*Nkx2.5* (*Hif1a*$^{f/f}$/*Nkx2.5*$^{Cre/+}$) mutant embryos at E12.5.

(B) E12.5 control (upper panels) and mutant (lower panels) heart sections stained with hematoxylin and eosin (H&E). Scale bars, 100 μm (overview) and 20 μm (insets).

(C) H&E quantification of ventricular walls and interventricular septum width in E12.5 control (black bars, n = 4) and mutant (white bars, n = 3) embryos.

(D) Quantification of BrdU immunostaining, represented as percentage of BrdU^{+} cells in the compact myocardium and trabeculae of E12.5 control (black) and *Hif1a*/*Nkx2.5* mutant (white) embryos (n = 3). In all graphs, bars represent mean ± SEM, Student's t test, n.s: non-significant. LV: left ventricle; RV: right ventricle; IVS: interventricular septum. Similar amount of male and female embryos has been used in these analyses.

progenitor-specific Cre recombinase driver *Nkx2.5*Cre (*Hif1a*$^{flox/flox}$/*Nkx2.5*$^{Cre/+}$, from here on *Hif1a*/*Nkx2.5*). Cre-mediated recombination was analyzed by agarose gel electrophoresis of cardiac and non-cardiac tissue at E12.5 (Figure S1A). A 400-bp product, corresponding to the processed *Hif1a* allele was only obtained in cardiac tissue in the presence of Cre recombinase activity, indicating that the deletion is specific of cardiac tissue and there is no ectopic recombination. To confirm deletion efficiency, we analyzed the expression of the floxed *Hif1a* exon by qPCR at E14.5, confirming its correct elimination despite a signal increase outside of the floxed region, probably caused by compensatory mechanisms (Figure S1B). Furthermore, *Phd3*, whose expression is dependent on HIF1, showed decreased expression in the *Hif1a*/*Nkx2.5* mutants (Figure S1B). We also determined HIF1α protein distribution and abundance within cardiac tissue by immunostaining in mutant and control littermates by E12.5 (Figure S1C). *Hif1a* deletion in the mutant embryos resulted in reduced HIF1α staining, with a displacement of the HIF1α channel intensity curve to lower fluorescence intensity (Figure S1D). It is noteworthy that deletion efficiency, as measured by qPCR, was higher than that estimated by immunostaining. This is probably because the mutant *Hif1a* mRNA produced after Cre recombination is sufficiently stable to be translated, although the resulting protein is not functional as it lacks the DNA-binding domain located in the N-terminal region of HIF1α. Efficient deletion was further confirmed by western blot of *Hif1a*-deficient heart lysates at E12.5 (Figure 1A). The lower molecular weight of the HIF1α protein band confirms the presence of a truncated protein in mutant embryos, which is recognized by HIF1 antibodies raised against the C-terminal domain.

Hif1a/*Nkx2.5* mutants were viable and recovered in the expected Mendelian proportions from E14.5 to weaning (Table 1). Histological analysis of control and *Hif1a*/*Nkx2.5* mutant hearts at E12.5 (Figure 1B) did not reveal differences between genotypes in terms of ventricular wall thickness (Figure 1C) or chamber sphericity (data not shown). Proliferation analysis by bromodeoxyuridine (BrdU) staining at E12.5 proved comparable proliferation index between control and *Hif1a*-deficient hearts (Figure 1D). Similar results were obtained at E14.5, when *Hif1a*-deficient embryos showed neither morphological alterations nor differences between genotypes in terms of cell size and proliferation by means of BrdU staining (data not shown). These results indicate that the lack of *Hif1a* in Nkx2.5 cardiac progenitors does not influence

Table 1. Analysis of *Hif1a/Nkx2.5* mutant embryo recovery

Stage	*Hif1a*$^{f/f}$/*Nkx2.5*$^{Cre/+}$	Total	Litters	Observed %	Expected %	p value
E14.5	20	90	13	24.4 ± 4.9	25	0.905
Weaning	10	38	6	28.6 ± 5.8	25	0.787

For each stage, table shows the number of mutant embryos recovered, the total number of embryos/pups collected, and the number of litters analyzed. The percentage of recovered mutants and the expected recovery percentage (25% in all cases) were compared by the Wilcoxon signed rank test. Equivalent proportion of male and female embryos and mice has been considered in the analysis.

cardiomyocyte proliferation and suggest that HIF1 signaling in this cell population is dispensable for proper cardiac development.

Embryonic loss of *Hif1a* in Nkx2.5 progenitors does not influence adult cardiac function or morphology

Albeit deletion of *Hif1a* in Nkx2.5 cardiovascular progenitors did not hamper embryonic ventricular chamber formation, we wondered whether mutant mice might develop heart alterations in the adulthood. Histology analysis by hematoxylin-eosin staining at five months of age did not indicate evident changes in cardiac morphology of *Hif1a*-deficient hearts relative to control animals (Figure 2A). Moreover, Masson's trichrome staining analysis excluded the presence of fibrotic areas in any of the genotypes (Figure 2B). Nevertheless, the lack of macroscopic malformations does not rule out that cardiac performance could be affected. To determine if embryonic deletion of *Hif1a* influences cardiac function during adulthood, we performed echocardiography in 5-month-old control and mutant mice. Both 2D and M mode analysis (Figure 2C) and the quantification of several morphological parameters confirmed the absence of anatomical alterations (Figures 2D and 2E). Furthermore, conserved cardiac function in *Hif1a/Nkx2.5* mutant versus control mice was demonstrated by means of ejection fraction and fractional shortening (Figure 2F). On the other hand, electrocardiographic analysis showed normal PR and QRS segment length in *Hif1a/Nkx2.5* mice (data not shown), ruling out the existence of conduction or coupling defects.

These results indicate that active HIF1 signaling in cardiovascular Nkx2.5 progenitors during heart development is not required for proper cardiac morphogenesis or normal heart function in the adulthood.

Cardiac deletion of *Hif1a* prevents the expression of glycolytic enzymes in the compact myocardium

To investigate the adaptive mechanisms operating upon *Hif1a* loss in Nkx2.5 cardiovascular progenitors to allow normal cardiac development, we performed massive expression analysis by RNA sequencing (RNA-seq) of E12.5 ventricular tissue from control and *Hif1a/Nkx2.5* mutant embryos. Subsequent bioinformatics analysis identified 14,406 genes being expressed. Among them, 201 genes showed differential expression: 118 were downregulated in mutant hearts relative to control hearts and 83 were upregulated, representing positively and negatively regulated targets respectively, dependent on functional HIF1 signaling in direct or indirect fashion (Table S1). To obtain a summarized view of their function, the list of 201 genes was subjected to enrichment analyses, which found significant associations with several metabolic processes, such as nucleotide/nucleoside and monocarboxylic acid metabolism, amino acid metabolism, and, especially, carbohydrate metabolism. Complete results are presented in Table S2, and a selection of significantly enriched processes is shown in Figure 3A, connected with the subset of differentially expressed genes that are involved in those processes. We have previously described the existence of metabolic territories in the embryonic myocardium with an enhanced glycolytic signature in the compact myocardium by E12.5 (Menendez-Montes et al., 2016). Here we found that glucose transporter 1 (GLUT1) protein levels were significantly reduced in the compact myocardium of the *Hif1a/Nkx2.5* mutant embryos by E12.5 (Figure 3B). Because Nkx2.5 cardiac progenitors contribute to different cardiac layers including myocardium, epicardium, and endocardium, to determine if the glycolytic inhibition observed in the *Hif1a/Nkx2.5* mutant embryos was associated with *Hif1a* loss in the myocardial layer, we specifically deleted *Hif1a* in cardiomyocytes using *cTnT*-Cre (Jiao et al., 2003) (*Hif1a*$^{flox/flox}$/*cTnT*$^{Cre/+}$, hereon *Hif1a/cTnT*). *Hif1a/cTnT* mutants also showed reduced HIF1α levels by E14.5 without cardiac developmental defects compared with control littermates (data not shown). The inhibition of the glycolytic program in both *Hif1a/Nkx2.5* and *Hif1a/cTnT* mutants was further confirmed by mRNA expression analysis of the critical enzymes *Glut1*, *Pdk1*, and *Ldha* by *in situ* hybridization at E12.5 (Figure 3C) and E14.5 (data not shown) in controls and *Hif1a* mutants. Results

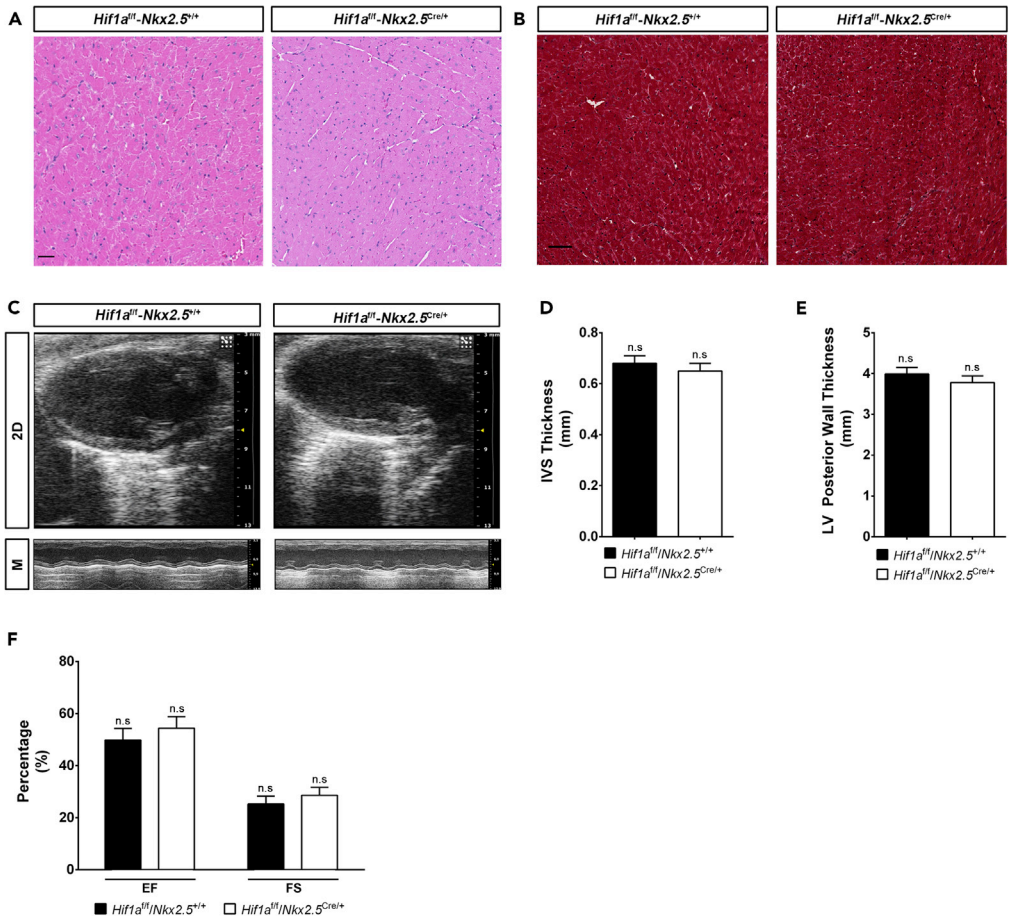

Figure 2. Cardiac morphology and function in adult *Hif1a/Nkx2.5* mutants

(A and B) H&E (A) and Masson's trichrome (B) staining of the left ventricle from a representative 5-month-old control (*Hif1a*$^{f/f}$/*Nkx2*$^{r+/+}$) and *Hif1a/Nkx2.5* mutant (*Hif1a*$^{f/f}$/*Nkx2.5*$^{Cre/+}$) heart. Even distribution of male and female mice was used in each experimental group (n = 6 females and 6 males). No differences associated with sex were observed in cardiac structure or fibrosis.

(C) Representative echocardiography imaging of 5-month-old control and *Hif1a*-deficient mutant mice in 2D mode (upper panels) and M mode (lower panels).

(D and E) Echocardiography-based quantification of interventricular septum (IVS) thickness (D) and left ventricle (LV) posterior wall thickness (E) in controls (black bars, n = 9) and *Hif1a/Nkx2.5* mutants (white bars, n = 11) by 5 months of age.

(F) Quantification of ejection fraction (EF) and fractional shortening (FS) in controls (black bars, n = 9) and *Hif1a/Nkx2.5* mutants (white bars, n = 11) by 5 months of age. Uniform distribution of male and female mice was used in each experimental group (n = 10 females and 10 males). No differences associated with sex were observed for cardiac structural or functional parameters. In all graphs bars represent mean ± SEM, Student's t test, n.s: non-significant. For all images, scale bars, 50 μm.

showed strong inhibition of glycolytic gene expression in the compact myocardium of *Hif1a*-deficient hearts at both stages. This sustained glycolytic inhibition at E14.5 was further validated by qPCR in both genetic models (Figures 3D and 3E), including the downregulation of *Slc16a3*, responsible for the transport of monocarboxylic acids, such as lactate, across mitochondrial membrane.

Taken together, these results confirm our previous findings that HIF1 signaling controls the expression of glycolytic genes in the embryonic heart and indicate that an active glycolytic program in the compact myocardium is not essential for proper cardiogenesis.

Lipid metabolism is preserved in cardiac *Hif1a* mutant mice

We have previously reported that sustained HIF1 signaling in the embryonic myocardium results in severe alterations of mitochondrial amount and function (Menendez-Montes et al., 2016). To evaluate the

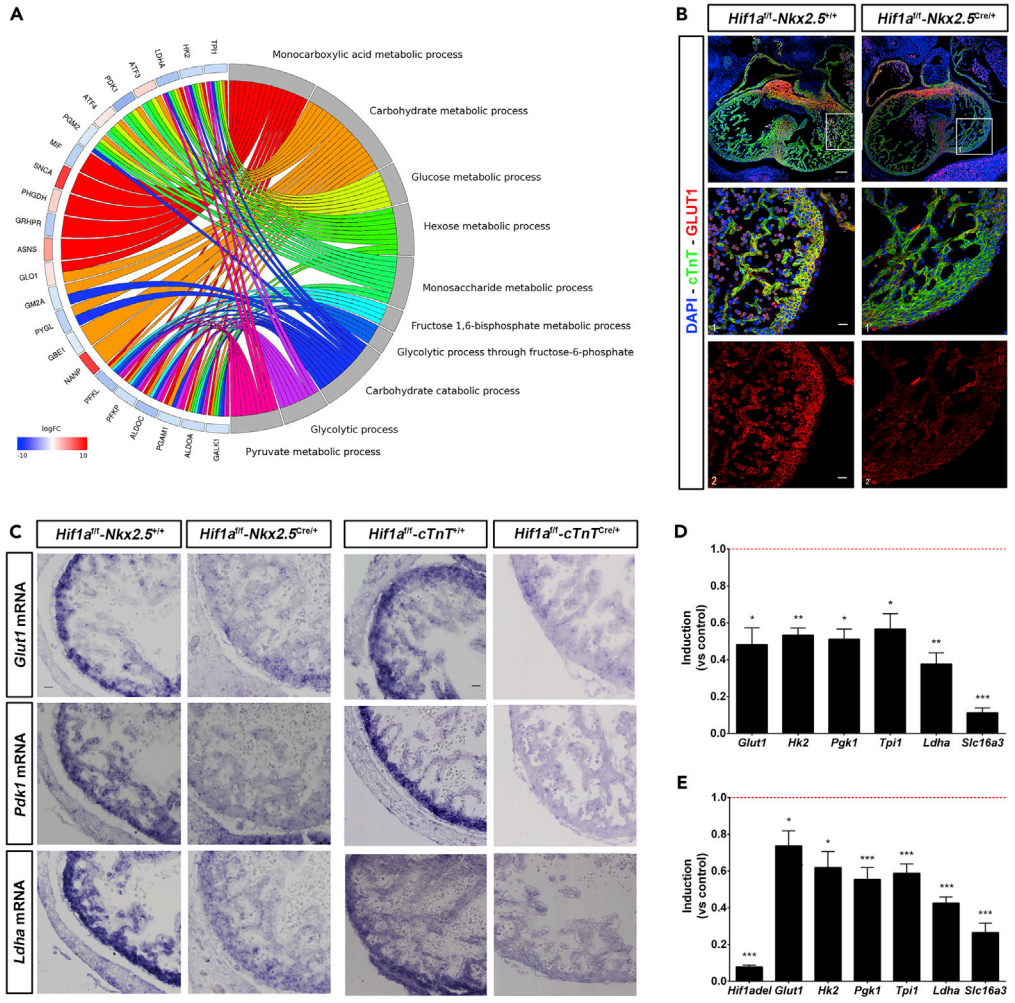

Figure 3. Glycolytic metabolism alterations in cardiac *Hif1a*-deficient embryos

(A) Circular plot representing logFC value for genes detected as differentially expressed in mutant (*Hif1a*$^{f/f}$/*Nkx2.5*$^{Cre/+}$) embryos, relative to controls (*Hif1a*$^{f/f}$/*Nkx2.5*$^{+/+}$), at E12.5 (left side), associated to Gene Ontology (GO) terms related to carbohydrate metabolism, selected among those detected as enriched with p value < 0.001 with GOrilla (right side). logFC values for genes are color coded: blue color denotes lower expression in mutant samples. Ribbons connecting genes and biological processes are colored by process.

(B) Representative GLUT1 immunofluorescence on E12.5 heart sections of controls (left panels) and *Hif1a/Nkx2.5* mutants (right panels). Nuclei shown in blue, Troponin T in green, and GLUT1 in red. Insets show left ventricle. Scale bars, 100 μm and 20 μm in insets.

(C) E12.5 *in situ* hybridization of *Glut1* (top panels), *Pdk1* (middle panels), and *Ldha* (bottom panels) in control and *Hif1a/Nkx2.5* mutant right ventricles (left) and in control and *Hif1a/cTnT* mutant right ventricles (right). Scale bar, 20μm

(D and E) RT-qPCR analysis of glycolytic genes from E14.5 *Hif1a/Nkx2.5* (D) and *Hif1a/cTnT* (E) mutant ventricles. Bars (mean ± SEM, n = 3) represent fold induction relative to baseline expression in littermate controls (red line). Student's t test. *p value<0.05; **0.005<p value<0.01, ***p value<0.005. Equivalent proportion of male and female embryos have been included in all experiments.

bioenergetics adaptations in response to the lack of cardiac HIF1 activation we investigated mitochondrial network and activity in *Hif1a/NKx2.5* mutants. Analysis and quantification of ventricular ultrastructure by transmission electron microscopy at E12.5 indicated a moderate increase in mitochondrial content in *Hif1a*-deficient embryos compared with control littermates. Images also confirmed our previously reported observation that mitochondrial number is higher in the trabecular layer than in the compact myocardial layer (Menendez-Montes et al., 2016), both in control and *Hif1a/Nkx2.5* mutant hearts (Figure 4A). Enriched mitochondrial content in *Hif1a/NKx2.5* mutants correlated with reduced expression levels of HIF1 target

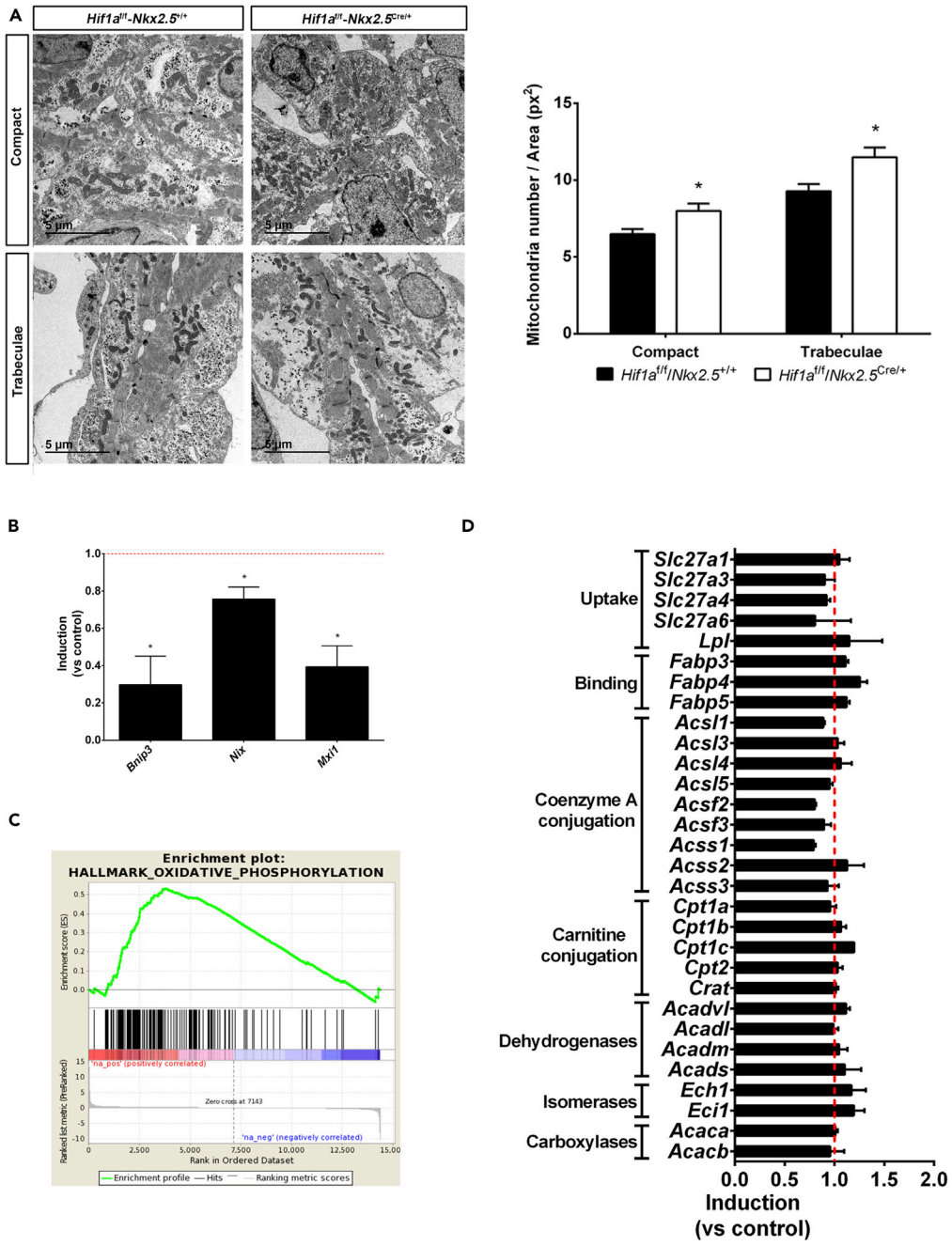

Figure 4. Mitochondrial content and lipid metabolism in *Hif1a/Nkx2.5* mutants at E12.5

(A) Transmission electron micrographs of ventricular tissue from a representative E12.5 control embryo (*Hif1a*$^{f/f}$/*Nkx2.5*$^{+/+}$, left) and a mutant littermate (*Hif1a*$^{f/f}$/*Nkx2.5*$^{Cre/+}$, right), showing compact myocardium (top panels) and trabeculae (bottom panels), and quantification of total mitochondria in electron micrographs from E12.5 controls (black bars) and mutants (white bars). Results are expressed as number of mitochondria per tissue area (px^2). Scale bars, 5 µm. Bars represent mean ± SEM (n = 4). Student's t test, *p value<0.05

(B) RT-qPCR analysis of mitophagy-related genes in E12.5 *Hif1a/Nkx2.5* mutant ventricles. Bars (mean ± SEM, n = 3 for *Bnip3* and *Mxi1* and n = 4 for *Nix*) represent fold induction relative to baseline expression in littermate controls (red line). Student's t test, *p value<0.05.

(C) GSEA enrichment plot for the Hallmark database Oxidative Phosphorylation gene set. The red to blue stripe represents 14,406 genes detected as expressed after differential expression analysis, ranked by logFC. Genes at the left side (colored in red) are more expressed in *Hif1a/Nkx2.5* mutants, and those located at the right side (colored in blue) are

Figure 4. *Continued*
more expressed in control littermates. Vertical black lines represent the position of members of the Oxidative Phosphorylation gene set along the ranked collection of genes. The green curve represents cumulative enrichment score.
(D) Fold change gene expression determined by RNA-seq of genes involved in fatty acid uptake and catabolism in *Hif1a/Nkx2.5* mutants. Red line represents baseline expression in control littermates. Bars represent mean ± SEM (n = 2). All experiments were performed using a comparable number of male and female embryos at each stage.

genes involved in mitophagy like *Nix* and *Bnip3* (Zhang et al., 2008) or genes that negatively regulate mitochondrial biogenesis through Myc transcriptional repression like *Mxi1 (*max interacting protein 1) (Figure 4B). Furthermore, we observed a significant enriched expression of genes related to oxidative phosphorylation determined by gene set enrichment analysis (Table S3, Figure 4C).

As mature cardiomyocytes rely on FA oxidation (FAO) for ATP production and cardiac performance, one possible metabolic adaptation of *Hif1a*-deficient hearts associated with increased mitochondrial content could be an early utilization of FA to provide sufficient ATP levels in the absence of effective glycolysis. However, RNA-seq (Figure 4D) and proteomic results (data not shown) demonstrated that the expression of genes involved in lipid catabolism was not different in control and Hif1a/Nkx2.5 genotypes, at E12.5. These results indicate that inhibited glycolysis due to *Hif1a* loss is not associated with a compensatory increase in FAO.

In summary, our observations demonstrate that reduced HIF1 signaling promotes an increment of cardiac mitochondrial network and suggest the activation of metabolic compensatory mechanisms other than FAO activation upon glycolytic inhibition in *Hif1a/Nkx2.5* mutant embryos.

Amino acid metabolic program is transiently enhanced in cardiac *Hif1a*-deficient embryos

As indicated earlier, enrichment analysis identified several metabolic processes that could be altered upon deletion of *Hif1a* in cardiovascular progenitors, some of them related with amino acid metabolism and, specifically, to the "cellular response to amino acid starvation" (Table S2). Complementary functional enrichment analyses allowed to pinpoint more precise functional terms, which suggested alterations in Ala, Leu, Val, Ile, Asn, Asp, Ser, and Gly biosynthesis (Figure 5A, Table S4). These results lead us to hypothesize about the activation of a metabolic reprogramming toward amino acid oxidative catabolism in embryonic cardiomyocytes in the absence of effective glycolysis associated with *Hif1a* deletion.

To validate this hypothesis, we performed global proteomic analysis in *Hif1a/Nkx2.5* embryos and control littermates by E12.5. Quantitative analyses revealed a significant increase in the abundance of proteins related to amino acid metabolism and, specifically, glutamine family metabolism (Figure 5B and Table S5). In addition, the decrease observed for proteins related to glycolysis confirmed the inhibited glycolytic gene expression program upon *Hif1a* deletion (Figure 3). Therefore, quantitative results for both gene expression, by RNA-seq, and protein abundance, by tandem mass spectrometry (MS/MS) proteomics, correlate to a certain extent, showing inhibited glycolysis (Figure 5C, left) and increased amino acid catabolism (Figure 5C, right). Specifically, *Hif1a/Nkx2.5* mutants showed increased expression and protein levels of genes contributing to anaplerosis of amino acids into Krebs cycle. These contributions (Figure S2) included aromatic amino acids (Phe, Tyr), polar amino acids (Asn, Asp, Gln, Glu, Ser, and Cys), Pro, Gly, and branched-chain amino acids (Val, Leu, and Ile). Urea cycle was also upregulated, resulting in increased contribution of Arg to Krebs cycle by the generation of fumarate, which can also act as a Krebs cycle intermediate. To determine differences between the amino acid profiles of *Hif1a/Nkx2.5* mutant and control hearts, we performed proton nuclear magnetic resonance (^{1}H-NMR) spectroscopy. The ventricular chambers of E12.5 *Hif1a/Nkx2.5* mutants showed higher levels of glutamine and total GLU (glutamine + glutamate) (Figures 5D and 5E). This metabolic signature is consistent with the *Hif1a/Nkx2.5* transcriptional and proteomic profiles. Finally, to investigate whether this amino acid signature was maintained over time in *Hif1*a-deficient hearts, we analyzed the expression levels of amino acid transporters by RT-qPCR at E14.5 and E17.5 (Figure 5F). The results showed that gene expression levels of several transporters, such as Slc7a5 (*Lat1)* (transporter of Trp, Phe, Tyr, and His, and also Met, Val, Leu, and Ile [Yanagida et al., 2001]), *Slc7a11* (transporter of Cys [Lim and Donaldson, 2011]), and *Slc3a2* (transporter of Val, Leu and Ile by association with *Slc7a5* [Kanai et al., 1998]), as well as the leucyl-tRNA synthetase *Lars,* were still upregulated by E14.5 in *Hif1a*-deficient hearts, but returned to control-like expression levels by E17.5.

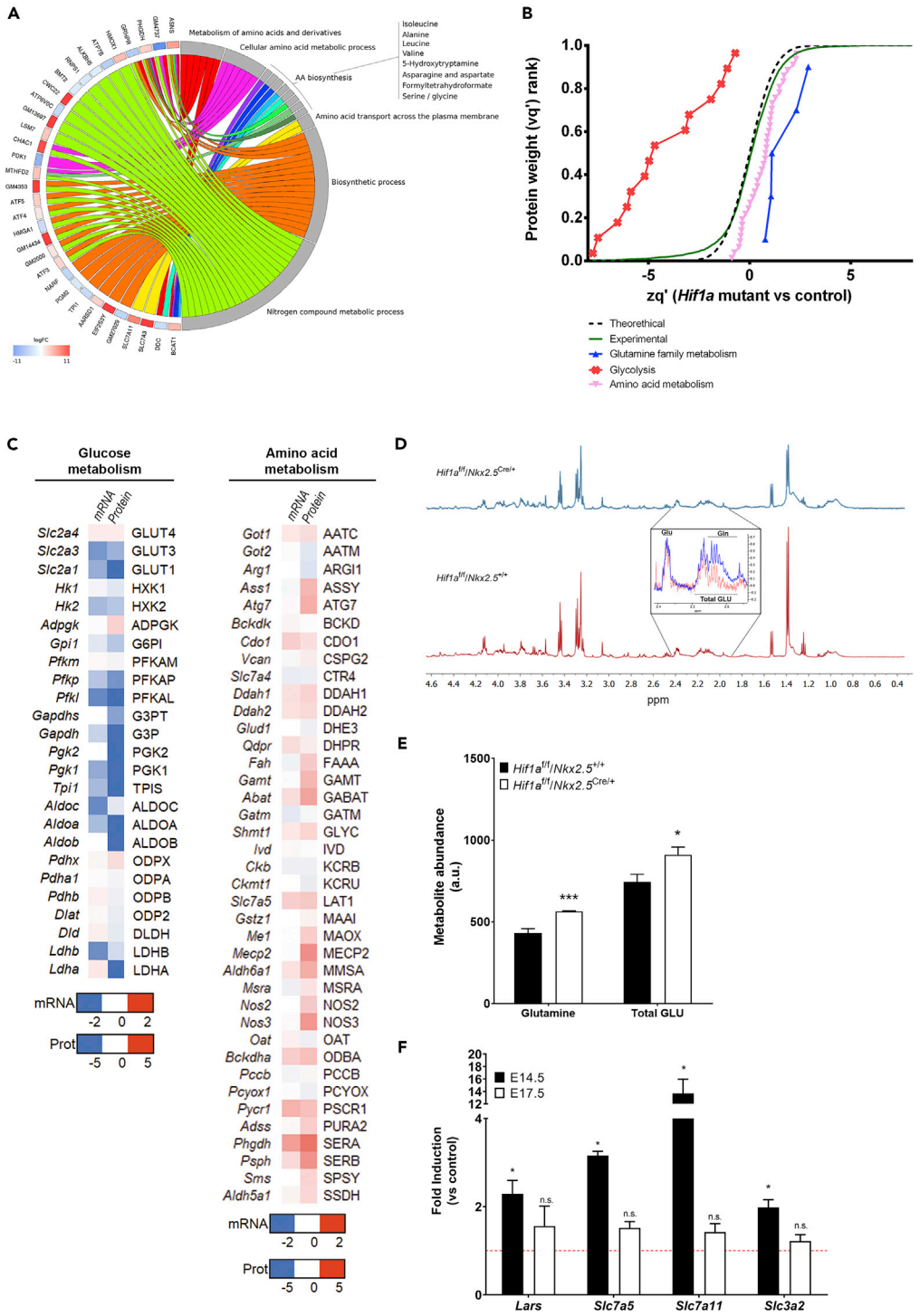

Figure 5. Metabolic adaptations in *Hif1a*-deficient hearts

(A) Circular plot representing logFC values for genes detected as differentially expressed in mutant ($Hif1a^{f/f}/Nkx2.5^{Cre/+}$) embryos, relative to controls ($Hif1a^{f/f}/Nkx2.5^{+/+}$) at E12.5 (left side), associated to a selection of functional terms related to amino acid metabolism (right side). Functions were detected with Panther by comparison against the Biological Process component of the Gene Ontology database, as well as against the Panther Pathway and Reactome databases. All functional terms were enriched with p value < 0.05. logFC values are color coded: red color denotes higher expression in mutant samples. Ribbons connecting genes and functional terms are colored by process.

Figure 5. *Continued*

(B) Representation of protein statistical weights (wq') grouped by functional categories (FDR<1%, n = 6) versus protein abundance in *Hif1a*-deficient hearts relative to control embryos (zq') at E12.5, as determined by MS/MS proteomics. A displacement right from the experimental curve indicates increased pathway in mutant embryos, whereas a left displacement represents a reduction.

(C) Heatmap representation of mRNA (quantified by RNA-seq) and protein (quantified by MS/MS) of components of glucose (left) and amino acid (right) metabolic pathways. Color code indicated in the legend is calculated as the value found in *Hif1a/Nkx2.5* mutants relative to control littermates.

(D) Representative ^{1}H-NMR spectra in ventricular samples from E12.5 control (bottom) and *Hif1a/Nkx2.5* mutant embryos (top). The inset highlights the differences in glutamine and total GLU [glutamine (Gln) + glutamate (Glu)] NMR signals.

(E and F) (E) ^{1}H-NMR spectroscopy quantification of glutamine and total GLU abundance in control (black) and *Hif1a/Nkx2.5* mutant embryos (white). Bars represent mean ± SEM (n = 3). (F) RT-qPCR analysis of amino acid transporter gene expression in *Hif1a* mutant ventricular tissue at E14.5 (black bars) and E17.5 (white bars). Bars (mean ± SEM, n = 2–4 for E14.5 and n = 3 for E17.5) represent fold induction relative to baseline expression in littermate controls (red line). For all graphs, Student's t test, *p value<0.05, ***p value<0.005, n.s. non-significant. Even proportion of male and female embryos has been included to carry out these experiments at each gestational stage.

These data indicate that upregulation of amino acid transport is transient and suggest that temporary increase of amino acid catabolism and anaplerosis could act as a compensatory mechanism to overcome the loss of glycolytic metabolism upon *Hif1a* loss until the FAO is established later in gestation, reflecting the metabolic flexibility of the embryonic heart to adapt to different substrates for energy supply.

ATF4 signaling is upregulated in *Hif1a/Nkx2.5* mutant embryos

The fact that there is a transient upregulation of general amino acid catabolism upon *Hif1a* loss in cardiovascular progenitors suggests the existence of upstream regulators that are temporally induced in the *Hif1a/Nkx2.5* mutants. Amino acid metabolism and its transport is tightly regulated through several pathways, including mTOR (mammalian target of rapamycin), GCN2 (general control non-derepresable 29), and ATF4 (Activating Transcription Factor 4), among others (Bröer and Bröer, 2017). Upstream regulator analysis of our RNA-seq data using Ingenuity Pathway Analysis (IPA) in fact shows that ATF4 and CHOP could function as main regulators of a gene set implicated in amino acid metabolism in *Hif1a*-deficient hearts (Figure 6A and Table S6). ATF4 is a transcriptional regulator that activates the expression of genes involved in amino acid transport and metabolism (Harding et al., 2003) and also responds to nutrient and metabolic stress in hypoxia (Weidemann and Johnson, 2007). *Atf4* gene expression, and mRNA levels of its target genes, such as *Slc7a11, Slc7a3, Asns, Lars,* or *Trib3,* among others, are upregulated in our *Hif1a/Nkx2.5* deletion model by E12.5 (Figure 6B). Furthermore, ATF4 protein levels were increased at E12.5 and E14.5 in cardiac lysates from *Hif1a/Nkx2.5* mutant hearts compared with control littermates (Figure 6C). Interestingly, transcriptional upregulation of ATF4 is sustained at E14.5, but its expression returned to control levels by E17.5 (Figure 6D), following an expression pattern similar to that of amino acid transporters (Figure 5F). Because glucose deprivation upon glycolytic inhibition conditions is known to promote the activation of unfolded protein response (UPR) (Badiola et al., 2011; Ikesugi et al., 2006; Vavilis et al., 2016), we decided to examine the expression levels of genes involved in UPR in the *Hif1a/Nkx2.5* mutant versus control hearts. The results show a significant upregulation in the expression of genes involved in UPR such as ATF3, ATF4, or CHAC1 among others (Figure 6E).

All together these results led us to suggest that *Hif1a* loss in cardiovascular progenitors induces the temporal activation of ATF4 expression and ATF4-mediated amino acid response probably trough UPR activation in response to glycolytic impairment.

Loss of *Hif1a* in Nkx2.5 progenitors leads to transient induction of HIF2 by midgestation

In the absence of active HIF1 cascade, HIF2α, an alternative HIFα isoform able to form functional heterodimers with ARNT, could play a compensatory role. To explore this possibility, we analyzed HIF2α abundance by western blot and found protein expression induction by E12.5 in the *Hif1a/Nkx2.5*-deficient hearts and comparable levels by E14.5 relative to controls (Figures 7A and 7B). A similar induced expression by E12.5 was observed for the HIF2 target gene, PAI-1 (plasminogen activator inhibitor 1) (Figures 7C and 7D). Interestingly, glucose deprivation has been shown to activate HIF2 signaling in an acetylation-dependent manner (Chen et al., 2015). We hypothesize that this adaptive activation of HIF2 signaling could partially contribute together with ATF4 upregulation to the transcriptional induction of amino acid transporters observed in the cardiac *Hif1a/Nkx2.5*-deficient model. Indeed, HIF2α has been involved in the

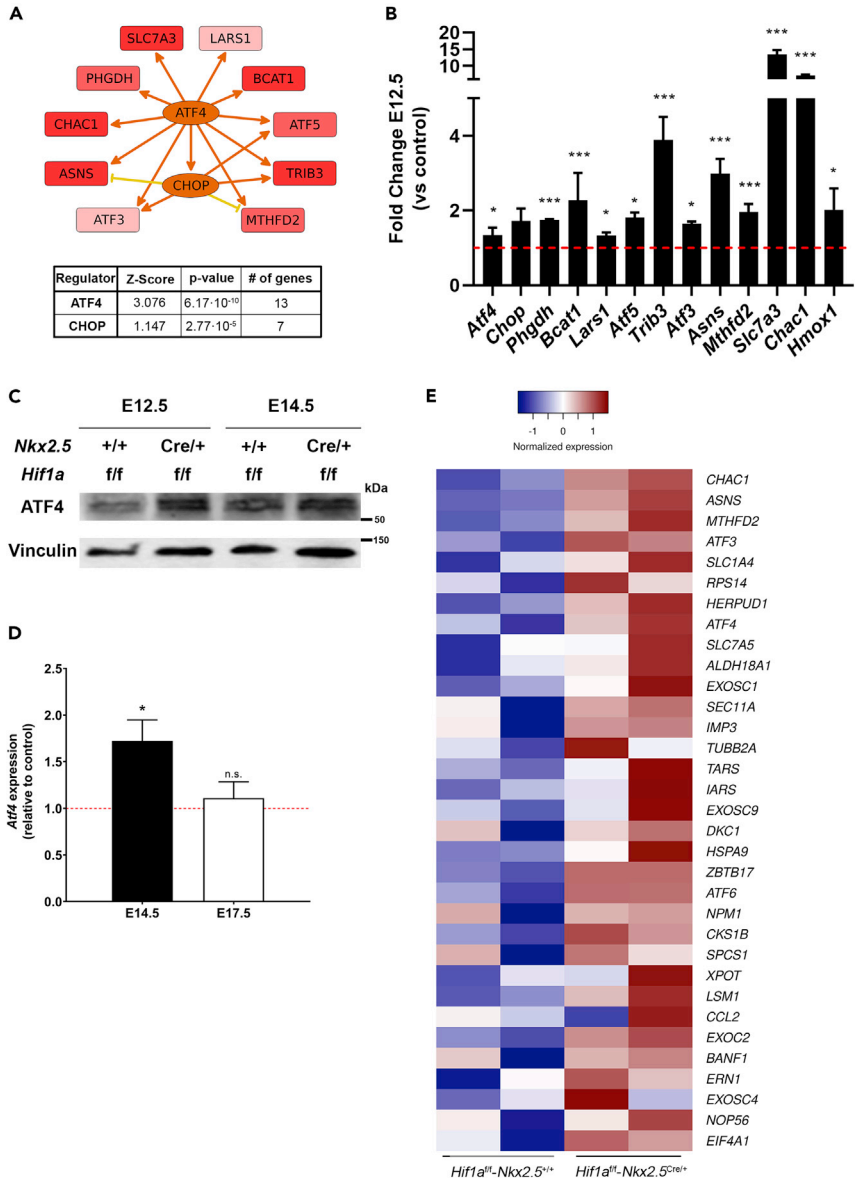

Figure 6. Upstream regulators of amino acid catabolism activation in *Hif1a*-deficient hearts

(A) Regulatory network summarizing the interactions between ATF4 and CHOP with a collection of genes related to amino acid metabolism, detected as differentially expressed at E12.5 in *Hif1a/Nkx2.5*-deficient hearts relative to controls. The graph is a simplified version of a mechanistic network predicted after IPA's upstream regulator analysis on the complete set of 201 differentially expressed genes. Intensity of red color in target genes is proportional to logFC. Intensity of orange color in regulator genes (ATF4 and CHOP) is proportional to the predicted activation *Z* score. Arrow-pointed and flat-headed lines represent positive and negative regulation interactions, respectively. Orange and yellow lines represent congruent and non-congruent connections, respectively, relative to the predicted activation state of regulators. The inset below summarizes *Z* score value and enrichment p value for ATF4 and CHOP, as well as the number of differentially expressed genes that are regulated by each of them.

(B) Relative expression of genes related to amino acid metabolism downstream of ATF4 determined by RNA-seq at E12.5 in *Hif1a/Nkx2.5* mutant versus control ventricles (n = 2). Student's t test. *p value<0.05, *** p value<0.005.

(C) Representative immunoblot out of 5 against ATF4 (upper panel) and Vinculin (lower panel) from ventricular heart lysates of control ($Hif1a^{f/f}/Nkx2.5^{+/+}$) and *Hif1a/Nkx2.5* mutant ($Hif1a^{f/f}/Nkx2.5^{Cre/+}$) embryos at E12.5 and E14.5.

(D) RT-qPCR analysis of *Atf4* gene expression at E14.5 (black bar) and E17.5 (white bar) in *Hif1a/Nkx2.5* mutant ventricular tissue. Bars (mean ± SEM, n = 5 for E14.5 and n = 3 for E17.5) represent fold induction relative to baseline expression in littermate controls (red line). Student's t test, * p value<0.05, n.s. non-significant.

Figure 6. *Continued*
(E) Heatmap representing RNA-seq based, normalized expression levels for genes involved in the unfolded protein response (UPR). The UPR gene set, as defined in the Hallmark database, was detected as enriched in mutant embryos after GSEA, although enrichment was not statistically significant (nominal p value = 0.31). Genes presented in the heatmap correspond to the leading-edge subset, this is, those mostly contributing to the calculated enrichment score. All experiments and analyses were performed using equivalent amount of male and female embryos at each stage.

direct control of *Slc7a5* (Lat1) expression by binding to the proximal promoter of the gene in renal clear cell carcinoma, as well as in lung, liver, and glioblastoma cells (GBCs) (Corbet et al., 2014; Elorza et al., 2012; Zhang et al., 2020). Additionally, HIF2 signaling has been related to the expression of other amino acid metabolism-related genes that are increased in *Hif1a/Nkx2.5* mutants compared with controls, such as *Mthfd2* or *Atf3* (Green et al., 2019; Turchi et al., 2008). Hence, these results suggest that HIF2 could further participate in the metabolic reprogramming toward amino acid catabolic pathways in the absence of effective HIF1 signaling.

In summary, our data demonstrate that HIF1 signaling in Nkx2.5 cardiac progenitors and cardiomyocytes is dispensable for proper heart formation and that the absence of *Hif1a* triggers a cardiac metabolic reprogramming, enhancing temporal amino acid catabolism to ensure sufficient ATP and biosynthetic precursors to sustain cardiac growth and function even in the absence of glycolysis (Figure 7E). Importantly, these adaptations might be relevant in the adulthood under pathological scenarios associated with oxygen signaling like pulmonary hypertension or cardiomyopathy toward the development of novel drugs against new metabolic targets.

DISCUSSION

Here, we describe that *Hif1a* loss in Nkx2.5 cardiovascular progenitors or cardiomyocytes causes glycolytic program inhibition in the compact myocardium (CM) by E12.5, without compromising normal cardiac development and embryonic viability. Our results show that upon *Hif1a* deletion, the embryonic myocardium conserves FAO capacity but exhibits the ability to activate metabolic programs oriented to amino acid catabolism, together with an increase in the mitochondrial content by E12.5. Taken together, our findings point out the metabolic versatility of the embryonic heart and conciliate the discrepancies from previous deletion models of *Hif1a* in cardiovascular progenitors.

Integration with previous *Hif1a* deletion model in the embryonic heart

As outlined in the introduction, there is a lack of consensus between previous reports on cardiac embryonic mouse models of *Hif1a* loss (Guimarães-Camboa et al., 2015; Huang et al., 2004; Krishnan et al., 2008). The *Hif1a* haploinsufficiency of some of these models outside the heart Nkx2.5 territories might cause extracardiac affections, such as vascular or placental, that could significantly influence the described phenotype. Indeed, the use of a *Hif1a*-null allele has been reported to cause cardiovascular malformations associated with maternal diabetes (Bohuslavova et al., 2013). In this regard, the exhaustive characterization by Guimaraes-Camboa et al. at gene expression level extensively overlaps with our RNA-seq data, except in terms of stress and apoptotic pathways, upregulated only in the null-allele context of their mutant.

Moreover, we have also analyzed a *Hif1a* null/floxed model in Nkx2.5 progenitors in parallel with the homozygous floxed model described here. We found that although glycolytic inhibition by E14.5 is comparable in both models (data not shown), only the null/floxed mice exhibited embryonic lethality (5% retrieved versus 25% expected, p value 0.0029, n = 7 litters), in contrast with the observed viability for the homozygous floxed mice. This observation, together with other results, supports the notion that cardiac HIF1 is dispensable for heart development, although an extensive comparison, in terms of gene expression in placental and vascular embryonic tissue, between the homozygous floxed and the null/floxed models would be necessary to exclude extracardiac influences of *Hif1a* deficiency affecting heart development as reported by Guimaraes-Camboa and colleagues, and also observed by the lab of Steven Fisher using a global conditional *Hif1a* knockout mice (Kenchegowda et al., 2014).

Amino acid catabolism and metabolic versatility of the embryonic heart

A key finding of our investigation is the fact that the embryonic myocardium is able to upregulate alternative metabolic pathways (amino acids transportation and catabolism), and to promote mitochondrial enrichment that could support the ATP demand upon glycolytic inhibition subsequent to *Hif1a* loss. The

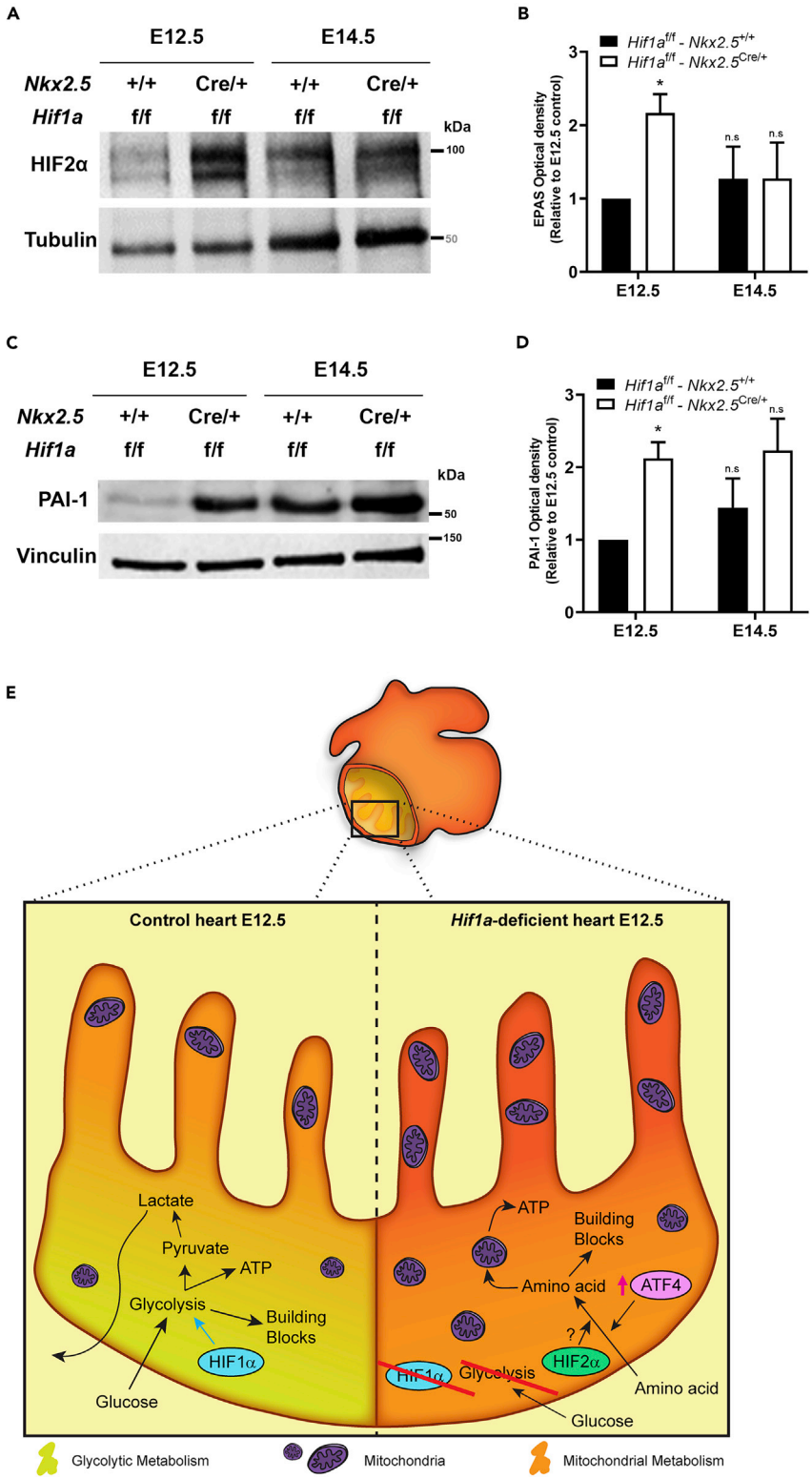

Figure 7. HIF2 signaling induction upon *Hif1a* deletion

(A) Representative immunoblot against HIF2α (upper panel) and Tubulin (lower panel) in heart lysates of control (*Hif1a*$^{f/f}$/*Nkx2.5*$^{+/+}$) and *Hif1a*/*Nkx2.5* mutant (*Hif1a*$^{f/f}$/*Nkx2.5*$^{Cre/+}$) embryos at E12.5 and E14.5.

(B) Quantification of HIF2α band intensity normalized by Tubulin as loading control (n = 3).

Figure 7. *Continued*

(C) Representative immunoblot against PAI-1 (upper panel) and Vinculin (lower panel) in heart lysates of control (*Hif1a*$^{f/f}$/*Nkx2.5*$^{+/+}$) and *Hif1a*/*Nkx2.5* mutant (*Hif1a*$^{f/f}$/*Nkx2.5*$^{Cre/+}$) embryos at E12.5 and E14.5.

(D) Quantification of PAI-1 band intensity normalized by Vinculin as loading control (n = 3). For all graphs, bars (mean ± SEM, n = 3) represent fold induction relative to baseline expression in littermate controls at E12.5 or E14.5. Student's t test. *p value<0.05, n.s: non-significant. Comparable proportion of male and female embryos has been included to perform these experiments at each gestational stage.

(E) Model representing the embryonic myocardium by E12.5. Compact myocardium is mainly glycolytic (yellowish) by the action of HIF1 signaling, whereas trabeculae rely more on mitochondrial metabolism (orange) in control embryos (left). In *Hif1a* mutants (right), glycolysis is compromised and the whole myocardium relies on mitochondrial metabolism, displaying higher mitochondrial content, and favoring the use of amino acids as energy source parallel to the activation of ATF4 and HIF2 signaling.

use of amino acids as cardiac metabolic fuel has been proposed mainly in oxygen-deprived scenarios (Bing et al., 1954; Julia et al., 1990). Amino acids provide, by deamination, carbon skeletons that can be converted into pyruvate, alpha-ketoglutarate, succinyl-CoA, fumarate, oxalacetate, acetyl-CoA, and acetoacetyl-CoA, all of them metabolites that can be incorporated into the Krebs cycle (Evans and Heather, 2016; Neubauer, 2007). As detailed earlier, our cardiac *Hif1a*-deficient model upregulates, both at the transcriptional and protein levels, a variety of amino acid transporters and biosynthetic and catabolic enzymes, which can replenish the Krebs cycle upon glucose deprivation. Moreover, the fact that this upregulation is accompanied by an increase in mitochondrial content indicates that the embryonic heart, in the absence of *Hif1a*, readapts its metabolism to maintain enough ATP levels and building blocks, without compromising the normal protein synthesis required for myocardium development and embryo viability.

Interestingly, this adaptation is transient and reversible, as revealed by the control-like levels of amino acid transporters and *Atf4* transcripts found at later stages by E17.5, without precluding the embryonic metabolic switch toward FAO previously described (Menendez-Montes et al., 2016). These observations indicate that the embryonic myocardium has the plasticity to modulate its metabolism to adapt to the energetic demand and nutrient availability. Moreover, in addition to this interesting role of amino acid catabolism activation in the embryonic context, the use of amino acids as an alternative energy source could be an attracting option to achieve cardioprotection and recovery after cardiac injury. In this regard, some of the enzymes upregulated in our massive screenings in *Hif1a*-deficient hearts are involved in Ser biosynthesis and one-carbon cycle, including *Phgdh, Psph,* and *Shmt1*. These pathways have been previously described to increase glutathione levels and protect the heart against oxidative stress (Zhou et al., 2017), also in a context of myocardial hypertrophy (Padrón-Barthe et al., 2018).

Origin of catabolized amino acids in *Hif1a*-deficient hearts

An interesting open aspect of the metabolic adaptation exhibited by the *Hif1a*-deficient hearts is the source of amino acid supply during glycolytic inhibition upon *Hif1a* loss. In this regard, two potential sources could be considered. First, protein-forming amino acids could be recycled through autophagy. This hypothesis is reasonable considering the context of the embryonic heart, where protein turnover, especially transcription factors, occurs fast and at a high rate (Merz et al., 1981). Moreover, a positive nitrogen balance has been reported in both adult rat and human hearts, indicative of rapid turnover of tissue proteins (Sprinson and Rittenberg, 1949). Interestingly, our *Hif1a* mutant embryos showed increased transcription of *p62,* a cargo-recognizing protein involved in autophagic degradation of cellular proteins (Lim et al., 2015). Although an extensive characterization analyzing autophagy, pro- and anti-autophagic signaling pathways, and protein labeling and turnover would be needed to further investigate this hypothesis, the fact that autophagy could be involved in this metabolic adaptation suggests an exciting link between cardiac metabolism, hypoxia, and autophagy.

Another possible source of amino acids in *Hif1a*-deficient hearts is fetal circulation. Even though an extensive characterization of fetal blood nutrient content over gestation has not been reported, the transcriptional increase in several membrane amino acid transporters observed in *Hif1a/Nkx2.5* mutants suggests that *Hif1a*-deficient cardiomyocytes could be obtaining amino acids directly from embryonic circulation. Interestingly, cardiac amino acids uptake in human subjects infused intravenously with protein hydrolysate increases by 245% (Bing et al., 1954), showing that the heart can respond to blood amino acids levels. Moreover, the regulation of amino acid transporters' expression in the placenta is essential for maintaining high levels of amino acids in the fetal blood to sustain embryo growth (Díaz et al., 2014). In this regard, an

increased cardiac uptake of amino acids in the *Hif1a*-deficient embryo could result in increased amino acids supply through the placenta that might respond to some secreted cues in the absence of cardiac HIF1 signaling.

Molecular determinants of amino acid catabolism activation

Amino acid metabolism and transport is tightly regulated through several pathways, including mTOR, GCN2, and G-protein-coupled receptors, among others (Bröer and Bröer, 2017). ATF4 is a transcriptional regulator that activates the expression of genes involved in amino acid transport and metabolism (Harding et al., 2003) and also responds to nutrient and metabolic stress in hypoxia (Weidemann and Johnson, 2007). *Atf4* gene expression is positively regulated in the *Hif1a/Nkx2.5* deletion model at both transcriptional and protein levels. In addition, upstream regulators' analysis identified ATF4 and CHOP (*Ddit3*) as putative regulators of amino acid metabolism in *Hif1a*-deficient hearts. ATF4 is an essential factor for amino acid starvation, by activating the gene expression of genes containing amino acid response elements (AARE) (Zhang et al., 2010) and regulates CHOP expression (Averous et al., 2004).

Loss of HIF1α signaling results in downregulated expression of glycolytic enzymes. Glucose deprivation, in turn, has been shown to cause activation of UPR (Badiola et al., 2011; Ikesugi et al., 2006; Vavilis et al., 2016). In our *Hif1a* deletion model, reduced glycolysis was accompanied by increased expression of UPR genes, suggesting that *Hif1a* deletion could contribute to ATF4 activation through glycolytic inhibition and UPR activation in the embryonic myocardium.

Interestingly, the *Hif1a* deletion model by Guimarães-Camboa et al. (2015) also shows increased ATF4 signaling in *Hif1a*-deficient hearts, supporting ATF4 as one of the main regulators of the described metabolic adaptation upon loss of effective glycolysis in *Hif1a*-deficient hearts. Moreover, as ATF4 is upregulated in both animal models, and considering the lack of lethality of our floxed/floxed mice despite an efficient Cre-mediated recombination of *Hif1a* floxed exon 2, the upregulation of ATF4 does not seem to be responsible for the embryonic lethality reported by Zambon's/Evan's groups that, in contrast, reported the activation of p53 stress pathway. Further analysis of p53-associated effects in the *Hif1a* null/floxed mice, as well as extracardiac impact of elimination of one *Hif1a* copy in the germ line might contribute to understand the phenotype of null/floxed mice.

Previous work in renal clear cell carcinoma, liver, and lung has identified a novel axis connecting HIF2 with mTOR through the action of the L-type amino acid transporter LAT1 (Elorza et al., 2012). Furthermore, mTORC1 has been reported to activate purine synthesis through the activation of ATF4 via a cellular stress-independent mechanism (Ben-Sahra et al., 2016). Hence, we hypothesized that upregulation of HIF2α in the *Hif1a/Nkx2.5* mutant hearts might lead to the activation of mTOR pathway that could further connect with ATF4 activation. However, analysis of the phosphorylation state of mTOR targets Factor 4E Binding Protein (4EBP1) and S6 Kinase (S6K) by western blot and immunohistochemistry revealed inhibition of these downstream effectors of mTOR in the *Hif1a/Nkx2.5* mutant hearts (data not shown), demonstrating that HIF2/LAT1/mTOR axis is not conserved in the embryonic myocardium and suggesting that ATF4 upregulation occurs in a HIF1 and mTORC1-independent manner, probably associated to enhanced UPR activation due to impaired glycolysis.

We also show that *Hif1a/Nkx2.5* mutants display higher levels of glutamine and glutamate compared with controls. Both amino acids are important carbon and nitrogen sources that can be used for energy production as well as for nucleotide and protein synthesis in cancer cells. In some tissues like the brain, part of glutamate can arise from branched-chain amino acids like leucine, isoleucine, or valine, which are transported into the cytosol via L-type amino acid transporters (LAT1-4) and converted into branched-chain alpha ketoacids through the action of cytosolic (BCAT1) or mitochondrial (BCAT2) branched-chain aminotransferases (Yudkoff, 1997). A recent article on GBCs describes the regulation of branched-chain amino acid reprogramming by HIFs and shows that the main LAT isoform expressed in GBC is LAT1. The authors show that Lat1 promoter can be transactivated by both HIF1 and HIF2, although BCAT1, associated to GBC proliferation, is only regulated by HIF1 in this cell type (Zhang et al., 2020). In contrast, in the *Hif1a/Nkx2.5* mutant hearts we have observed upregulation of LAT1 and BACT1 independently of HIF1 abrogation, suggesting that in the embryonic heart HIF2 might play an important role in controlling the expression of these key elements of BCAA metabolic reprogramming. Further functional and molecular characterization of HIF1/HIF2 double mutant mice would contribute to confirm this hypothesis. Another important aspect

for future research would be to determine the relative contribution of HIF2 versus ATF4 in the amino acid metabolic reprogramming observed in the *Hif1a/Nkx2.5* mutant mice as both transcription factors share several common target genes related to amino acid transport and catabolism.

In summary, our work demonstrates that HIF1 elimination in cardiac progenitors and cardiomyocytes is dispensable for heart development and function, and that impaired glycolysis during cardiogenesis in *Hif1a*-deficient mice induces a transient reprogramming of amino acid metabolism concomitant with HIF2 and ATF4 activation. These observations uncover the metabolic flexibility of the embryonic heart that might share common adaptive bioenergetics responses to cancer cells under compromised glucose and FAO availability.

Limitations of the study

Performing metabolic flow studies during embryonic development is challenging as metabolites can be utilized by the maternal metabolism before reaching the embryo. Hence, future functional assays on amino acids utilization will contribute to reinforce our transcriptomic and proteomic data on amino acids import and catabolism activation.

The definitive role of ATF4 and HIF2 in metabolic reprogramming to amino acid catabolism in the absence of glycolytic program in the *Hif1a* cKO will require future genetic analysis of single and double knockout models.

Resource availability

Lead contact

Further information and requests for resources and reagents should be directed to and will be fulfilled by the Lead Contact, Silvia Martín-Puig (silvia.martin@cnic.es; silvia.martin@ufv.es).

Materials availability

Mouse lines generated in this study are available upon request from the Lead Contact with a completed Materials Transfer Agreement and might require additional payment.

Data and code availability

RNA-seq data have been deposited in NCBI's Gene Expression Omnibus (https://www.ncbi.nlm.nih.gov/geo) and are accessible through GEO Series accession number GSE164453.

Proteomic datasets (raw files, protein databases, search parameters, and results) have been deposited in the Peptide Atlas repository (http://www.peptideatlas.org) and are available through the accession number PASS01236.

METHODS

All methods can be found in the accompanying Transparent Methods supplemental file.

SUPPLEMENTAL INFORMATION

Supplemental Information can be found online at https://doi.org/10.1016/j.isci.2021.102124.

ACKNOWLEDGMENTS

The authors thank Lorena Flores for echocardiography technical assistance, Raquel Baeza and Mercedes de la Cueva for animal housing and handling, and CNIC Microscopy, Genomics and Histology Core Facilities for technical assistance. We thank Miguel Torres Sanchez, Jose Antonio Enriquez, Luke Szweda, and Hesham Sadek for critical discussion of the manuscript. This project has been supported by Fundación Centro Nacional de Investigaciones Cardiovasculares Carlos III (CNIC), Spain and by grants to S.M.-P. from the European Research Council, European Union, FP7-PEOPLE-2010-RG_276891; Fundación TV3 La Marató, Spain, 201507.30.31; Comunidad de Madrid (CAM); Spain and European Union (EU), B2017/BMD-3875; Instituto de Salud Carlos III, Spain, PI17/01817 cofunded by European Regional Development Fund (ERDF); Universidad Francisco de Vitoria (UFV), Spain and LeDucq Foundation, France, 17CVD04. I.M.-M. was supported by La Caixa-CNIC and Fundacion Alfonso Martín Escudero fellowships, Spain.

T.A.-G. was supported by a predoctoral award granted by CAM/EU and UFV, Spain, PEJD-2018-PRE/SAL-9529 and SM-P by a Contrato de Investigadores Miguel Servet (CPII16/00050) and UFV, Spain.

AUTHOR CONTRIBUTIONS

S.M.-P. conceived and supervised the project. I.M.-M. performed most of the *in vitro* and *in vivo* experiments with assistance from B.E., B.P., and T.A.-G., prepared the figures, and together with S.M.-P. analyzed the data and co-wrote the manuscript. M.J.G. performed all bioinformatic analysis and contributed to manuscript editing and discussion. E.B. and J.V. performed proteomic analysis. A.V.A. and L.J.J.-B. carried out echocardiographic studies. J.L.I.-G., A.F., and J.R.-C. performed metabolic analysis. Funding acquisition by S.M.-P.

DECLARATION OF INTERESTS

The authors declare no competing interests.

Received: July 1, 2020
Revised: December 1, 2020
Accepted: January 26, 2021
Published: February 19, 2021

REFERENCES

Averous, J., Bruhat, A., Jousse, C., Carraro, V., Thiel, G., and Fafournoux, P. (2004). Induction of CHOP expression by amino acid limitation requires both ATF4 expression and ATF2 phosphorylation. J. Biol. Chem. *279*, 5288–5297.

Badiola, N., Penas, C., Miñano-Molina, A., Barneda-Zahonero, B., Fadó, R., Sánchez-Opazo, G., Comella, J.X., Sabriá, J., Zhu, C., Blomgren, K., et al. (2011). Induction of ER stress in response to oxygen-glucose deprivation of cortical cultures involves the activation of the PERK and IRE-1 pathways and of caspase-12. Cell Death Dis. *2*, e149.

Ben-Sahra, I., Hoxhaj, G., Ricoult, S.J.H., Asara, J.M., and Manning, B.D. (2016). mTORC1 induces purine synthesis through control of the mitochondrial tetrahydrofolate cycle. Science *351*, 728–733.

Bing, R.J., Siegel, A., Ungar, I., and Gilbert, M. (1954). Metabolism of the human heart: II. Studies on fat, ketone and amino acid metabolism. Am. J. Med. *16*, 504–515.

Bohuslavova, R., Skvorova, L., Sedmera, D., Semenza, G.L., and Pavlinkova, G. (2013). Increased susceptibility of HIF-1α heterozygous-null mice to cardiovascular malformations associated with maternal diabetes. J. Mol. Cell. Cardiol. *60*, 129–141.

Bröer, S., and Bröer, A. (2017). Amino acid homeostasis and signalling in mammalian cells and organisms. Biochem. J. *474*, 1935–1963.

Cerychova, R., and Pavlinkova, G. (2018). HIF-1, metabolism, and diabetes in the embryonic and adult heart. Front. Endocrinol. (Lausanne) *9*, 460.

Chen, R., Xu, M., Nagati, J.S., Hogg, R.T., Das, A., Gerard, R.D., and Garcia, J.A. (2015). The acetate/ACSS2 switch regulates HIF-2 stress signaling in the tumor cell microenvironment. PLoS One *10*, e0116515.

Chung, S., Arrell, D.K., Faustino, R.S., Terzic, A., and Dzeja, P.P. (2010). Glycolytic network restructuring integral to the energetics of embryonic stem cell cardiac differentiation. J. Mol. Cell. Cardiol. *48*, 725–734.

Chung, S., Dzeja, P.P., Faustino, R.S., Perez-terzic, C., Behfar, A., and Terzic, A. (2011). Mitochondrial oxidative metabolism is required for the cardiac differentiation of stem cells. Natl. Institutes Heal. *4*, 1–12.

Corbet, C., Draoui, N., Polet, F., Pinto, A., Drozak, X., Riant, O., and Feron, O. (2014). The SIRT1/HIF2α axis drives reductive glutamine metabolism under chronic acidosis and alters tumor response to therapy. Cancer Res. *74*, 5507–5519.

Díaz, P., Powell, T.L., and Jansson, T. (2014). The role of placental nutrient sensing in maternal-fetal resource Allocation1. Biol. Reprod. *91*, 82.

Elorza, A., Soro-Arnáiz, I., Meléndez-Rodríguez, F., Rodríguez-Vaello, V., Marsboom, G., de Cárcer, G., Acosta-Iborra, B., Albacete-Albacete, L., Ordóñez, A., Serrano-Oviedo, L., et al. (2012). HIF2α acts as an mTORC1 activator through the amino acid carrier SLC7A5. Mol. Cell *48*, 681–691.

Evans, R.D., and Heather, L.C. (2016). Metabolic Pathways and Abnormalities (Surg. (United Kingdom)).

Fukuda, R., Zhang, H., Kim, J.W., Shimoda, L., Dang, C.V., and Semenza, G.L. (2007). HIF-1 regulates cytochrome oxidase subunits to optimize efficiency of respiration in hypoxic cells. Cell *129*, 111–122.

Green, N.H., Galvan, D.L., Badal, S.S., Chang, B.H., LeBleu, V.S., Long, J., Jonasch, E., and Danesh, F.R. (2019). MTHFD2 links RNA methylation to metabolic reprogramming in renal cell carcinoma. Oncogene *38*, 6211–6225.

Guimarães-Camboa, N., Stowe, J., Aneas, I., Sakabe, N., Cattaneo, P., Henderson, L., Kilberg, M.S., Johnson, R.S., Chen, J., McCulloch, A.D., et al. (2015). HIF1α represses cell stress pathways to allow proliferation of hypoxic fetal cardiomyocytes. Dev. Cell *33*, 507–521.

Harding, H.P., Zhang, Y., Zeng, H., Novoa, I., Lu, P.D., Calfon, M., Sadri, N., Yun, C., Popko, B., Paules, R., et al. (2003). An integrated stress response regulates amino acid metabolism and resistance to oxidative stress. Mol. Cell. *11*, 619–633.

Huang, Y., Hickey, R.P., Yeh, J.L., Liu, D., Dadak, A., Young, L.H., Johnson, R.S., and Giordano, F.J. (2004). Cardiac myocyte-specific HIF-1alpha deletion alters vascularization, energy availability, calcium flux, and contractility in the normoxic heart. FASEB J. *18*, 1138–1140.

Ikesugi, K., Mulhern, M.L., Madson, C.J., Hosoya, K.I., Terasaki, T., Kador, P.F., and Shinohara, T. (2006). Induction of endoplasmic reticulum stress in retinal pericytes by glucose deprivation. Curr. Eye Res. *31*, 947–953.

Jiang, B.H., Zheng, J.Z., Leung, S.W., Roe, R., and Semenza, G.L. (1997). Transactivation and inhibitory domains of hypoxia-inducible factor 1alpha. Modulation of transcriptional activity by oxygen tension. J. Biol. Chem. *272*, 19253–19260.

Jiao, K., Kulessa, H., Tompkins, K., Zhou, Y., Batts, L., Baldwin, H.S., and Hogan, B.L.M. (2003). An essential role of Bmp4 in the atrioventricular septation of the mouse heart service. Genes Dev. *17*, 2362–2367.

Julia, P., Young, H., Buckberg, G., Kofsky, E., and Bugyi, H. (1990). Studies of myocardial protection in the immature heart. II. Evidence for importance of amino acid metabolism in tolerance to ischemia. J. Thorac. Cardiovasc. Surg. *100*, 888–895.

Kaelin, W.G., and Ratcliffe, P.J. (2008). Oxygen sensing by metazoans: the central role of the HIF hydroxylase pathway. Mol. Cell *30*, 393–402.

Kanai, Y., Segawa, H., Miyamoto, K.I., Uchino, H., Takeda, E., and Endou, H. (1998). Expression cloning and characterization of a transporter for

large neutral amino acids activated by the heavy chain of 4F2 antigen (CD98). J. Biol. Chem. *273*, 23629–23632.

Kenchegowda, D., Liu, H., Thompson, K., Luo, L., Martin, S.S., and Fisher, S.A. (2014). Vulnerability of the developing heart to oxygen deprivation as a cause of congenital heart defects. J. Am. Heart Assoc. *3*, e000841.

Kim, J.W., Tchernyshyov, I., Semenza, G.L., and Dang, C.V. (2006). HIF-1-mediated expression of pyruvate dehydrogenase kinase: a metabolic switch required for cellular adaptation to hypoxia. Cell Metab. *3*, 177–185.

Krishnan, J., Ahuja, P., Bodenmann, S., Knapik, D., Perriard, E., Krek, W., and Perriard, J.-C. (2008). Essential role of developmentally activated hypoxia-inducible factor 1 for cardiac morphogenesis and function. Circ. Res. *103*, 1139–1146.

Lee, Y.M., Jeong, C.-H., Koo, S.-Y., Son, M.J., Song, H.S., Bae, S.-K., Raleigh, J.A., Chung, H.-Y., Yoo, M., and Kim, K.-W. (2001). Determination of hypoxic region by hypoxia marker in developing mouse embryos in vivo: a possible signal for vessel development. Dev. Dyn. *220*, 175–186.

Lei, L., Mason, S., Liu, D., Huang, Y., Marks, C., Hickey, R., Jovin, I.S., Pypaert, M., Johnson, R.S., and Giordano, F.J. (2008). Hypoxia-inducible factor-dependent degeneration, failure, and malignant transformation of the heart in the absence of the von Hippel-Lindau protein. Mol. Cell Biol. *28*, 3790–3803.

Lim, J., Lachenmayer, M.L., Wu, S., Liu, W., Kundu, M., Wang, R., Komatsu, M., Oh, Y.J., Zhao, Y., and Yue, Z. (2015). Proteotoxic stress induces phosphorylation of p62/SQSTM1 by ULK1 to regulate selective autophagic clearance of protein aggregates. PLoS Genet. *11*, e1004987.

Lim, J.C., and Donaldson, P.J. (2011). Focus on Molecules: the cystine/glutamate exchanger (System xc -). Exp. Eye Res. *92*, 162–163.

Llurba Olive, E., Xiao, E., Natale, D.R., and Fisher, S.A. (2018). Oxygen and lack of oxygen in fetal and placental development, feto–placental coupling, and congenital heart defects. Birth Defects Res. *110*, 1517–1530.

Lopaschuk, G.D., and Jaswal, J.S. (2010). Energy metabolic phenotype of the cardiomyocyte during development, differentiation, and postnatal maturation. J. Cardiovasc. Pharmacol. *56*, 130–140.

Majmundar, A.J., Wong, W.J., and Simon, M.C. (2010). Hypoxia-Inducible factors and the response to hypoxic stress. Mol. Cell *40*, 294–309.

Martin-Puig, S., Wang, Z., and Chien, K.R. (2008). Lives of a heart cell: tracing the origins of cardiac progenitors. Cell Stem Cell *2*, 320–331.

Menendez-Montes, I., Escobar, B., Palacios, B., Gómez, M.J., Izquierdo-Garcia, J.L., Flores, L., Jiménez-Borreguero, L.J., Aragones, J., Ruiz-Cabello, J., Torres, M., and Martin-Puig, S. (2016). Myocardial VHL-HIF signaling controls an embryonic metabolic switch essential for cardiac maturation. Dev. Cell *39*, 724–739.

Merz, E.A., Brinster, R.L., Brunner, S., and Chen, H.Y. (1981). Protein degradation during preimplantation development of the mouse. J. Reprod. Fertil. *61*, 415–418.

Moses, K.A., DeMayo, F., Braun, R.M., Reecy, J.L., and Schwartz, R.J. (2001). Embryonic expression of an Nkx2-5/Cre gene using ROSA26 reporter mice. Genesis *31*, 176–180.

Nanka, O., Krizova, P., Fikrle, M., Tuma, M., Blaha, M., Grim, M., and Sedmera, D. (2008). Abnormal myocardial and coronary vasculature development in experimental hypoxia. Anat. Rec. *291*, 1187–1199.

Neubauer, S. (2007). The failing heart–an engine out of fuel. N. Engl. J. Med. *356*, 1140–1151.

Padrón-Barthe, L., Villalba-Orero, M., Gómez-Salinero, J.M., Acín-Pérez, R., Cogliati, S., López-Olañeta, M., Ortiz-Sánchez, P., Bonzón-Kulichenko, E., Vázquez, J., García-Pavía, P., et al. (2018). Activation of serine one-carbon metabolism by calcineurin Aβ1 reduces myocardial hypertrophy and improves ventricular function. J. Am. Coll. Cardiol. *71*, 654–667.

Piao, L., Fang, Y.H., Parikh, K., Ryan, J.J., Toth, P.T., and Archer, S.L. (2013). Cardiac glutaminolysis: a maladaptive cancer metabolism pathway in the right ventricle in pulmonary hypertension. J. Mol. Med. *91*, 1185–1197.

Pouyssegur, J., Dayan, F., and Mazure, N.M. (2006). Hypoxia signalling in cancer and approaches to enforce tumour regression. Nature *441*, 437–443.

Puente, B.N., Kimura, W., Muralidhar, S.A., Moon, J., Amatruda, J.F., Phelps, K.L., Grinsfelder, D., Rothermel, B.A., Chen, R., Garcia, J.A., et al. (2014). The oxygen-rich postnatal environment induces cardiomyocyte cell-cycle arrest through DNA damage response. Cell *157*, 565–579.

Ream, M., Ray, A.M., Chandra, R., and Chikaraishi, D.M. (2008). Early fetal hypoxia leads to growth restriction and myocardial thinning. AJP Regul. Integr. Comp. Physiol. *295*, R583–R595.

Sprinson, D.B., and Rittenberg, D. (1949). The rate of utilization of ammonia for protein synthesis. J. Biol. Chem. *180*, 707–714.

Sugishita, Y., Watanabe, M., and Fisher, S.A. (2004). Role of myocardial hypoxia in the remodeling of the embryonic avian cardiac outflow tract. Dev. Biol. *267*, 294–308.

Turchi, L., Aberdam, E., Mazure, N., Pouysségur, J., Deckert, M., Kitajima, S., Aberdam, D., and Virolle, T. (2008). Hif-2alpha mediates UV-induced apoptosis through a novel ATF3-dependent death pathway. Cell Death Differ. *15*, 1472–1480.

Vavilis, T., Delivanoglou, N., Aggelidou, E., Stamoula, E., Mellidis, K., Kaidoglou, A., Cheva, A., Pourzitaki, C., Chatzimeletiou, K., Lazou, A., et al. (2016). Oxygen–glucose deprivation (OGD) modulates the unfolded protein response (UPR) and inflicts autophagy in a PC12 hypoxia cell line model. Cell. Mol. Neurobiol. *36*, 701–712.

Watanabe, Y., and Buckingham, M. (2010). The formation of the embryonic mouse heart: heart fields and myocardial cell lineages. Ann. N. Y. Acad. Sci. *1188*, 15–24.

Weidemann, A., and Johnson, R.S. (2007). A wrinkle in the unfolding of hypoxic response: HIF and ATF4. Blood *110*, 3492–3493.

Yanagida, O., Kanai, Y., Chairoungdua, A., Kim, D.K., Segawa, H., Nii, T., Cha, S.H., Matsuo, H., Fukushima, J., Fukasawa, Y., et al. (2001). Human L-type amino acid transporter 1 (LAT1): characterization of function and expression in tumor cell lines. Biochim. Biophys. Acta - Biomembr. *1514*, 291–302.

Yudkoff, M. (1997). Brain metabolism of branched-chain amino acids. Glia *21*, 92–98.

Yue, M., Jiang, J., Gao, P., Liu, H., and Qing, G. (2017). Oncogenic MYC activates a feedforward regulatory loop promoting essential amino acid metabolism and tumorigenesis. Cell Rep. *21*, 3819–3832.

Zhang, B., Chen, Y., Shi, X., Zhou, M., Bao, L., Hatanpaa, K.J., Patel, T., DeBerardinis, R.J., Wang, Y., and Luo, W. (2020). Regulation of branched-chain amino acid metabolism by hypoxia-inducible factor in glioblastoma. Cell. Mol. Life Sci. https://doi.org/10.1007/s00018-020-03483-1.

Zhang, H., Bosch-Marce, M., Shimoda, L.A., Tan, Y.S., Baek, J.H., Wesley, J.B., Gonzalez, F.J., and Semenza, G.L. (2008). Mitochondrial autophagy is an HIF-1-dependent adaptive metabolic response to hypoxia. J. Biol. Chem. *283*, 10892–10903.

Zhang, H., Gao, P., Fukuda, R., Kumar, G., Krishnamachary, B., Zeller, K.I., Dang, C.V., and Semenza, G.L. (2007). HIF-1 inhibits mitochondrial biogenesis and cellular respiration in VHL-deficient renal cell carcinoma by repression of C-MYC activity. Cancer Cell *11*, 407–420.

Zhang, Y., Jin, Y., Williams, T.A., Burtenshaw, S.M., Martyn, A.C., and Lu, R. (2010). Amino acid deprivation induces CREBZF/Zhangfei expression via an AARE-like element in the promoter. Biochem. Biophys. Res. Commun. *391*, 1352–1357.

Zhou, X., He, L., Wu, C., Zhang, Y., Wu, X., and Yin, Y. (2017). Serine alleviates oxidative stress via supporting glutathione synthesis and methionine cycle in mice. Mol. Nutr. Food Res. *61*.

iScience, Volume *24*

Supplemental information

Activation of amino acid metabolic program in cardiac HIF1-alpha-deficient mice

Ivan Menendez-Montes, Beatriz Escobar, Manuel J. Gomez, Teresa Albendea-Gomez, Beatriz Palacios, Elena Bonzon-Kulichenko, Jose Luis Izquierdo-Garcia, Ana Vanessa Alonso, Alessia Ferrarini, Luis Jesus Jimenez-Borreguero, Jesus Ruiz-Cabello, Jesus Vázquez, and Silvia Martin-Puig

TRANSPARENT METHODS

Animal care and housing

Hif1α$^{flox/flox}$ (Ryan et al., 2000)mice were maintained on the C57BL/6 background and crossed with mice carrying *Nkx2.5Cre* recombinase (Stanley et al., 2002) or *TnTCre* recombinase (Jiao et al., 2003) in heterozygosity. *Hif1α*$^{flox/flox}$ homozygous females were crossed with double heterozygous males and checked for plug formation. Mice were housed in SPF conditions at the CNIC Animal Facility. Welfare of animals used for experimental and other scientific purposes conformed to EU Directive 2010/63EU and Recommendation 2007/526/EC, enforced in Spanish law under Real Decreto 53/2013. Experiments with mice and embryos were approved by the authorized Environmental Department of Comunidad de Madrid, Spain, with reference numbers: PROEX 12/14 and PROEX 267/19.

Genotyping

Genotyping was performed using the following primers (Sigma Aldrich; USA) for *Hif1a floxed* alleles: 5' CGTGTGAGAAAACTTCTGGATG 3' and 5' AAAAGTATTGTGTTGGGGCAGT 3'. For *Hif1a* null allele: 5' GCCCATGGTAAGAGAGTAGGTGGG 3' and 5' 5' AAAAGTATTGTGTTGGGGCAGT 3'. For Cre alleles genotyping, *Nkx2.5*: 5' GCCCTGTCCCTCAGATTTCACACC 3', 5' GCGCACTCACTTTAATGGGAAGAG 3' and 5' GATGACTCTGGTCAGAGATACCTG 3' and *cTnT*: 5' TACTCAAGAACTACGGGCTGC 3' and 5' GCACTCCAGCTTGGTTCCCGA 3'.

Embryo extraction

Embryos at E12.5, E14.5 and E17.5 were extracted after pregnant female euthanasia by CO_2 inhalation and head and liver were removed. Equivalent proportion of male and female embryos have been included in all experiments. After dissection, embryos were snap frozen in liquid nitrogen for biochemical studies or fixed overnight at 4ºC in 4% PFA solution (RT15710, Electron Microscopy Sciences; USA). After fixation, embryos were dehydrated in ethanol series, embedded in paraffin and sectioned at 5µm for immunostaining and histological purposes and at 10µm for *in situ* hybridization.

Histological and immunohistochemical analysis

Histological sample processing and immunostaining was performed as described elsewhere (Menendez-Montes et al., 2016). Briefly, 5µm-thick paraffin sections were stained with hematoxylin &eosin (HE) following standard histological procedures at the CNIC Histopathology Facility. For adult cardiac tissue H&E and Masson Trichrome staining analysis, even distribution of male and female mice was used in each experimental group. No differences associated with sex were observed in structure or fibrosis. For immunostaining, sections were rehydrated, and antigens were retrieved by incubation in citrate buffer (10 mM sodium citrate, 0.05% Tween20, pH 6) in a pressure cooker. Sections were permeabilized with 0.5% Triton-X100 for 10 min and blocked with 10% goat serum (GS) (Cat. No. 16210-072, Life Technologies; NY; USA). Sections were incubated with primary antibodies in 10% GS overnight at 4ºC. After several washes with PBS-T, sections were incubated with secondary antibody (Life Technologies; NY; USA or Dako; Denmark) in 5% bovine serum albumin (BSA) for 1h at room temperature in the dark. When necessary, signal was amplified using fluorochrome-conjugated streptavidin (Life Technologies; NY; USA) for 1h at room temperature in the dark, or with the TSA System (Perkin Elmer; MA; USA). Finally, sections were incubated with DAPI (Millipore, MA; USA) and mounted in Fluorescent Mounting Medium (S3023, Dako, Denmark). Images were acquired with Zeiss

LSM700 (Zeiss; Germany) or Nikon A1R (Nikon; Japan) confocal microscopes. The primary antibodies used in this study were: HIF1α (NB100-479, Novus Biologicals; USA and GTX30647, Genetex, USA); cTnT (CT3, Developmental Studies Hybridoma Bank; USA); BrdU (347580, BD Biosciences; USA); Cy3-conjugated Smooth Muscle Actin (C6198, Sigma Aldrich; USA) and GLUT1 (Cat. No. 07-1401, Millipore, USA).

Quantification of histological and immunostained sections

HE staining was quantified as previously reported (Menendez-Montes et al., 2016) using ImageJ (Rasband, 2015). Briefly, images of HE-stained sections were acquired with a NanoZoomer-XR Digital slide scanner (Hamamatsu; Japan). Compact myocardium and IVS thickness and total width and height of ventricular chambers were measured using NDP View (Hamamatsu; Japan). Values of at least three independent litters were analyzed for significant statistical differences by Student's t test. For fluorescence intensity analysis in cardiomyocyte nuclei, our own pipeline for CellProfiler software was employed (Lamprecht et al., 2007). Briefly, cell nuclei were segmented and subsequently filtered by cTnT positive cytoplasmic staining. After filtering, HIF1α channel intensity was measured.

RNA extraction, cDNA synthesis and RT-qPCR

RNA extraction from embryonic hearts, cDNA synthesis and quantitative PCR were performed as previously described (Menendez-Montes et al., 2016). Primers are available under request. Briefly, total RNA was extracted using QiAzol Lysis Reagent (Qiagen; CA; USA) and the miRNeasy Mini Kit (Qiagen; CA; USA). Total amount of isolated RNA was retrotranscribed using the MultiScribe Reverse Transcriptase kit 8Applied Biosystems; CA; USA) and cDNA concentration was adjusted to 250ng/μL. All real-time qPCR reactions were performed in an AB7000 thermalcycler (Applied Biosystems; CA; USA) using SYBR Green PCR Master Mix (Applied Biosystems; CA; USA). Gene-specific primers were obtained from PrimerBank (http://pga.mgh.harvard.edu/primerbank/index.html) and checked for exon spanning using Primer3 (http://primer3.sourceforge.net/webif.php). Baseline normalization and thresholding were performed in automated mode with the SDS Software (Applied Biosystems; CA; USA). Cq values were analyzed using qBase (Biogazelle; Belgium) using 3 housekeeping genes (*GusB, Hprt* and *Rpl32*). Primer-specific efficiencies were tested with serial dilutions of control cDNA. Statistically significant differences between control and mutants were analyzed by Student's t test.

Probe synthesis and in situ hybridization

General probe synthesis, purification and in situ hybridization steps were followed according with our previous protocol (Menendez-Montes et al., 2016). Briefly, for anti-probe preparation, reverse primers carrying T7 polymerase promoter sequence at the 5' end were used. Amplified fragments were purified using QIAquick Gel Extraction Kit (Qiagen; CA; USA) and probes were transcribed using 100ng of the fragment and T7 polymerase in presence of DIG-labelled nucleotides (Roche, Switzerland) for 6h. Probes were treated with Dnase I and purified using illustra AutoSeq G50 Dye Terminator Removal kit (GE Healthcare, UK). For the probe synthesis, the following primers were used: *Glut1* 5' GGACTTTGATGGCTCCAGAA 3' and 5' GAGTGTCCGTGTCTTCAGCA 3', *Pdk1* 5' CTGGGTTTGGTTACGGATTG 3' and 5' GCCAGCTACTCCACGTTCTT 3' and *Ldha* 5' GGAAGGAGGTTCACAAGCAG 3' and 5' CTGCAGTTGGCAGTGTGTCT 3'.

For in situ hybridization staining, 10µm paraffin sections of embryos, stored at -20ºC, were rehydrated and subsequently post-fixed in 4% PFA. After this, mRNA was exposed by incubation with Proteinase K (0.01mg/mL) at 37ºC for 10 min, and masking proteins were denatured by incubation in 0.7N HCl for 15 min at room temperature. Sections were blocked with hybridization buffer (50% formamide, 25% SSC 20X pH 5.5, Denhardt's buffer 1X, 0.1% Tween20; Chaps 10% 0.01mL/L; 0.05g/L tRNA) and incubated overnight at 65ºC with DIG-labeled probe at a final concentration of 5µL/mL. After several washes in decreasingly stringent conditions, sections were incubated overnight at 4ºC with anti-DIG-AP Fab fragments (Roche; Switzerland). Finally, sections were conditioned in alkaline phosphatase buffer (NaCl 0.1M; MgCl2 0.05M; Tris-HCl 0.1M pH 9.5; 0.1% Tween20) and developed with BM Purple (Roche; Switzerland) at 37ºC for 1-4 days, until the signal was clear

Electron microscopy and micrograph quantification

Embryonic hearts were processed for transmission electron microscopy following the standard procedures. Briefly, after overnight fixation in 3% glutaraldehyde/4%PFA, samples were refixed in 1% osmium tetroxide and embedded in epoxy resin. 60nm sections were counterstained with uranyl acetate and lead citrate and imaged using a JEOL JEM1010 (100 KV) transmission electron microscope. Control and mutant embryonic hearts from three independent litters were analyzed. For quantification of mitochondria and lipid droplets, ten images of compact myocardium and ten of trabeculae were taken at 5000x magnification. Mitochondria and droplets were counted manually by blinded observers using the ImageJ CellCounter plugin. Values were normalized to the total tissue area, in pixels, excluding extracellular areas in the image.

Protein extraction and Western Blot

Embryonic hearts were homogenized using RIPA buffer and a TissueLyser in presence of protease and phosphatase inhibitors (Inhibitor cocktail (Roche, Switzerland) and 1µM sodium ortovanadate). After clarification by centrifugation, protein concentration was measured using Pierce BA Protein Assay kit (23227, Thermo Scientific; USA) following manufacturer instructions. 30µg of protein were denaturized at 95ºC for 5 min, loaded on an 8% polyacrylamide SDS-PAGE gel and run at 120V for 90min. Subsequently, samples were transferred to a nitrocellulose membrane by wet transfer at 400mA for 2h. Membranes were blocked with 5% BSA for 1h and incubated with primary antibodies O/N at 4ºC. Next day, membranes were washed in TBS-T buffer and incubated with the corresponding HRP-conjugated secondary antibodies (Dako, Denmark) at 1:5000 dilution for 1h at RT. After washing, signal was developed using ECL Primer Western Blotting Detection Reagent (Amersham; UK) and detected by a LAS-3000 imaging system (Fujifilm; USA). The primary antibodies used in this study were: anti-HIF2α[ep190b] (NB100-132, Novus Biologicals) dilution 1:200, anti-HIF1α (10006421, Cayman; USA) dilution 1:200, anti-PAI-1 (sc-5297, Santa Cruz) dilution1:500, anti-ATF4 (11815, Cell Signalling; USA) dilution 1:500, anti-vinculin (V4505, Sigma-Aldrich; USA) dilution1:5000 , anti-αtubulin[DM1A] (ab7291,Abcam; UK) dilution 1:1000 and anti-SMA cy3 (C6198, Sigma-Aldrich; USA) dilution 1:1000.

RNASeq and bioinformatics analysis of gene expression

RNASeq data processing and differential expression analyses (n=2 per group) were performed as previously described (Menendez-Montes et al., 2016): E12.5 ventricles were collected and total RNA was extracted as detailed above. RNA integrity was verified using Agilent 20100 Bioanalyzer (Agilent Technologies; CA; USA). Index-tagged cDNA libraries were constructed from 500ng total RNA using TruSeq RNA Sample Preparation v2 kit (Illumina; CA; USA). Libraries were quantified in a Q-bit fluorometer (Life Technologies; CA; USA). After normalization, libraries

were applied to an Illumina flow cell for cluster generation and sequencing-by-synthesis. Single reads of 75bp were generated following the standard RNA sequencing protocol. To produce fastq files, reads were processed using CASAVA package (Illumina; CA; USA).

For differential expression analysis, only genes expressed with at least at 1 count per million in at least in 2 samples were considered. Changes in gene expression were considered significant if associated with Benjamini-Hochberg adjusted P value < 0.055. Functional enrichment analyses were performed with Gorilla (Eden et al., 2009), Panther (Thomas et al., 2003), IPA (Qiagen, USA), REVIGO (Supek et al., 2011) and GSEA (Subramanian et al., 2005). Enriched functional terms were filtered by applying P value thresholds described in the corresponding Table or Figure captions. Circular plots summarizing logFC values for genes, and their association to enriched functional terms were generated with GO plot (Walter et al., 2015).

Magnetic resonance spectroscopy and data processing

E12.5 snap-frozen embryonic ventricles were processed and analyzed by High Resolution Magic-Angle Spinning (HR-MAS) Nuclear Magnetic Resonance Spectroscopy (^{1}H-NMR as previously described (Menendez-Montes et al., 2016). Briefly, intact heart tissue was placed in zirconium oxide rotor in the presence of 0.1mM Trimethylsilyl propanoic acid in deuterium water. Samples were acquired at 500.13 MHz using a Bruker AVIII 500 spectrometer at 11.7 T over 4 hours using a CPMG pulse sequence. Data processing was performed using the Metabonomic R package (Izquierdo-García et al., 2009, Röst et al., 2016, Gil-De-La-Fuente et al., 2019). Spectra were referenced to the TSP singlet at 0 ppm (parts per million) chemical shift.

Proteomics analysis

Proteins from pellets after metabolite extraction were pooled in groups of four, treated with 50mM iodoacetamide (IAM) and digested with trypsin using the Filter Aided Sample Preparation (FASP) digestion kit (Expedeon) (Wiśniewski et al., 2011) according to manufacturer's instructions. Dried peptides were labeled with iTRAQ-8plex according to manufacturer's instructions, desalted on OASIS HLB extraction cartidges (Waters Corp.), separated into 4 fractions using the high pH reversed-phase peptide fractionation kit (Thermo) and dried-down before MS analysis on an Orbitrap Fusion Tribrid mass spectrometer (Thermo Fisher Scientific, Bremen, Germany) (García-Marqués et al., 2016). Peptide identification, quantification and systems biology analysis was performed as in (García-Marqués et al., 2016) Significant abundance changes of proteins or homogeneous categories of KO mice compared to controls were detected at 1% FDR.

Adult mice echocardiography and analysis

5 months-old mice were anesthetized using 1.5% isoflurane at a flow rate of 1L/min. Once anesthetic plane was reached, cardiac images were acquired using a MS400 probe, at 30MHz for 2D and M mode images and 24MHz for Color and Pulsed Doppler modes, using an ultrasound scanner VEVO2100 (Visualsonics, Canada). Equal male and female mice were used in each experimental group. No differences associated with sex were observed for cardiac functional parameters.

Statistical analysis and data representation

For histological, immunohistochemical quantifications, electron microscopy and RT-qPCR, values were pooled for embryos with the same genotype from independent litters and analyzed by the indicated statistical test using SPSS software (IBM; USA), with statistical significance

assigned at P ≤0.05. Values were represented as mean±SEM using GraphPad Prism (GraphPad; USA).

SUPPLEMENTAL REFERENCES

Eden, E., Navon, R., Steinfeld, I., Lipson, D., Yakhini, Z., 2009. GOrilla: a tool for discovery and visualization of enriched GO terms in ranked gene lists. BMC Bioinformatics 10, 48.

García-Marqués, F., Trevisan-Herraz, M., Martínez-Martínez, S., Camafeita, E., Jorge, I., Lopez, J.A., Méndez-Barbero, N., Méndez-Ferrer, S., del Pozo, M.A., Ibáñez, B., Andrés, V., Sánchez-Madrid, F., Redondo, J.M., Bonzon-Kulichenko, E., Vázquez, J., 2016a. A Novel Systems-Biology Algorithm for the Analysis of Coordinated Protein Responses Using Quantitative Proteomics. Mol. Cell. Proteomics 15, 1740–1760.

Izquierdo-García, J.L., Rodríguez, I., Kyriazis, A., Villa, P., Barreiro, P., Desco, M., Ruiz-Cabello, J., 2009. A novel R-package graphic user interface for the analysis of metabonomic profiles. BMC Bioinformatics 10, 363.

Jiao, K., Kulessa, H., Tompkins, K., Zhou, Y., Batts, L., Baldwin, H.S., Hogan, B.L.M., 2003. An essential role of Bmp4 in the atrioventricular septation of the mouse heart service. Genes Dev. 17, 2362–2367.

Lamprecht, M.R., Sabatini, D.M., Carpenter, A.E., 2007. CellProfiler???: Free, versatile software for automated biological image analysis. Biotechniques 42, 71–75.

Menendez-Montes, I., Escobar, B., Palacios, B., Gómez, M.J., Izquierdo-Garcia, J.L., Flores, L., Jiménez-Borreguero, L.J., Aragones, J., Ruiz-Cabello, J., Torres, M., Martin-Puig, S., 2016. Myocardial VHL-HIF Signaling Controls an Embryonic Metabolic Switch Essential for Cardiac Maturation. Dev. Cell 39.

Rasband, W., 2015. ImageJ. U. S. Natl. Institutes Heal. Bethesda, Maryland, USA //imagej.nih.gov/ij/.

Ryan, H.E., Poloni, M., McNulty, W., Elson, D., Gassmann, M., Arbeit, J.M., Johnson, R.S., 2000. Hypoxia-inducible factor-1α is a positive factor in solid tumor growth. Cancer Res. 60, 4010–4015.

Stanley, E.G., Biben, C., Elefanty, A., Barnett, L., Koentgen, F., Robb, L., Harvey, R.P., 2002. Efficient Cre-mediated deletion in cardiac progenitor cells conferred by a 3'UTR-ires-Cre allele of the homeobox gene Nkx2-5. Int J Dev Biol 46, 431–439.

Subramanian, A., Tamayo, P., Mootha, V.K., Mukherjee, S., Ebert, B.L., Gillette, M.A., Paulovich, A., Pomeroy, S.L., Golub, T.R., Lander, E.S., Mesirov, J.P., 2005. Gene set enrichment analysis: A knowledge-based approach for interpreting genome-wide expression profiles. Proc. Natl. Acad. Sci. U. S. A.

Supek, F., Bošnjak, M., Škunca, N., Šmuc, T., 2011. Revigo summarizes and visualizes long lists of gene ontology terms. PLoS One.

Thomas, P.D., Campbell, M.J., Kejariwal, A., Mi, H., Karlak, B., Daverman, R., Diemer, K., Muruganujan, A., Narechania, A., 2003. PANTHER: A library of protein families and subfamilies indexed by function. Genome Res.

Walter, W., Sánchez-Cabo, F., Ricote, M., 2015. GOplot: an R package for visually combining

expression data with functional analysis. Bioinformatics 31, 2912–4.

Wiśniewski, J.R., Ostasiewicz, P., Mann, M., 2011. High recovery FASP applied to the proteomic analysis of microdissected formalin fixed paraffin embedded cancer tissues retrieves known colon cancer markers. J. Proteome Res. 10, 3040–3049.

SUPPLEMENTAL FIGURES

Supplemental Figure S1

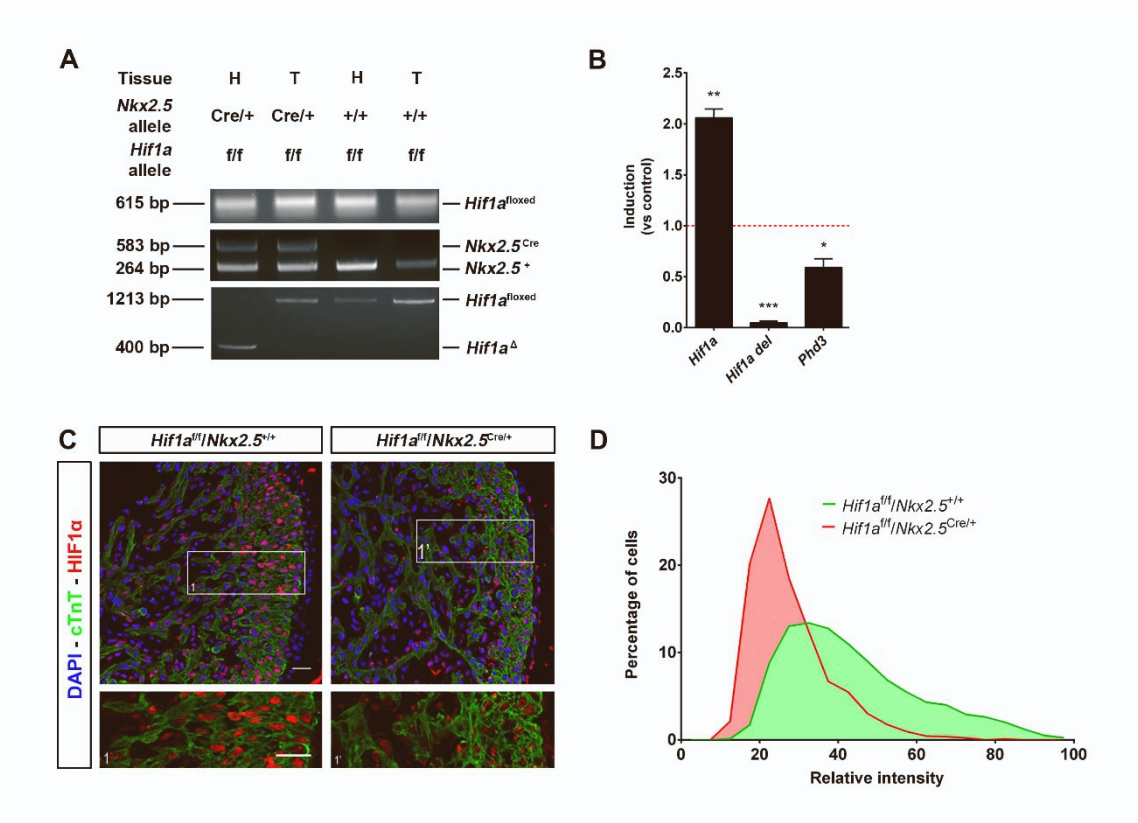

Figure S1. Deletion efficiency of *Hif1a*/*Nkx2.5* mutants.

Related to Figure 1.

A) Agarose electrophoresis showing PCR products from heart (H) and tail (T) tissue of E12.5 mutant embryos (*Hif1a*$^{f/f}$/*Nkx2*$^{rCre/+}$, lanes 1 and 2) and controls (*Hif1a*$^{f/f}$/*Nkx2.5*$^{+/+}$, lanes 3 and 4). Top gel: floxed (615 bp) allele of the *Hif1a* gene. Middle gel: wild-type (264 pb) and Cre (583 bp) alleles of the Nkx2.5 gene. Bottom gel: processed *Hif1a* allele after Cre-mediated recombination (400bp) and unprocessed allele (1213bp). **B)** RT-qPCR quantification of *Hif1a,* exon 2 (floxed) from *Hif1a* and *Phd3* transcripts in E14.5 *Hif1a*-mutant hearts. Bars (mean±SEM, n=3-6) represent fold induction relative to baseline expression in littermate controls (red line). *p-value<0.05; **0.01<p-value<0.05; ***p-value<0.005, Student's t test. **C)** HIF1α immunofluorescence at E12.5 in control and mutant embryos (Dapi staining shows nuclei in blue, Troponin T in green and HIF1α in red). Scale bars, 20µm. **D)** Representative analysis of cardiomyocyte HIF1α nuclear protein expression intensity, quantified by immunohistochemical staining of heart

sections from an E12.5 control embryo (green curve) and a *Hif1a*-null littermate (red curve).

Supplemental Figure S2

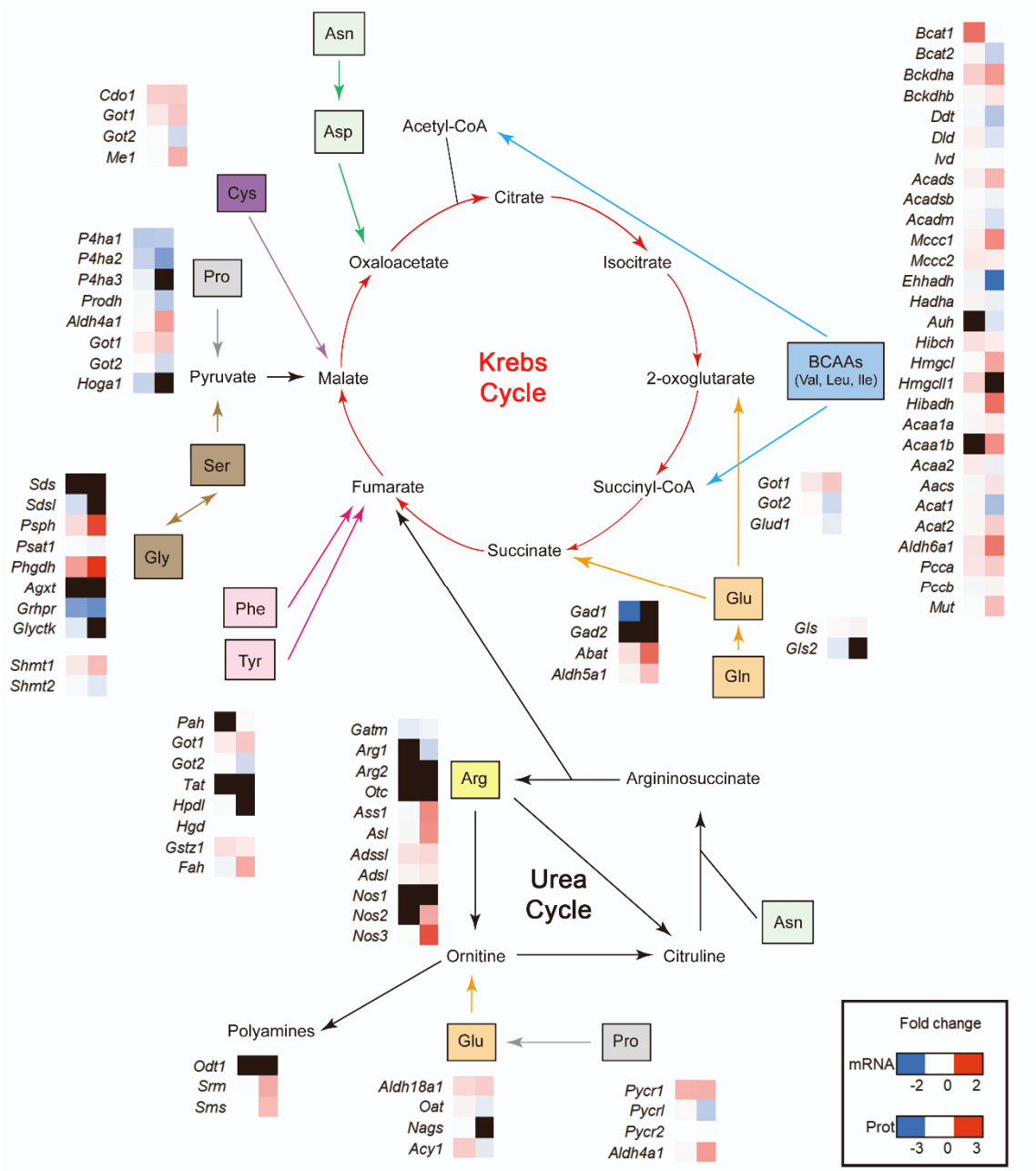

Figure S2. Schematic representation of amino acid contributions to Krebs and Urea Cycles. Related to Figure 5.

Schematic overview of the transcriptomics (mRNA expression, left column) and proteomics data (standardized protein quantifications, right column) of the re-wired metabolic pathways in the heart of *Hif1a*/*Nkx2.5* mutants (*Hif1a*$^{f/f}$/*Nkx2.5*$^{Cre/+}$) over control embryos (*Hif1a*$^{f/f}$/*Nkx2*$^{r+/+}$) at E12.5. Data are represented as individual heat maps for the transcript/protein of each pathway calculated as logarithmic Fold Change (logFC) and coded by color intensity following the scale at the bottom. ND indicates no detection. All 14406 expressed genes and 4276 quantified proteins were considered.